Using ARM Observations to Evaluate Climate Model Simulations of Land-Atmosphere Coupling on the U.S. Southern Great Plains

Thomas J. Phillips[1], Stephen A. Klein[1], Hsi-Yen Ma[1], Qi Tang[1], Shaocheng Xie[1], Ian N. Williams[2], Joseph A. Santanello[3], David R. Cook[4], and Margaret S. Torn[2]

[1]Lawrence Livermore National Laboratory
Livermore, California 94551

[2]Lawrence Berkeley National Laboratory
Berkeley, California 94720

[3]NASA Goddard Space Flight Center Hydrological Sciences Laboratory
Greenbelt, Maryland 20771

[4]Argonne National Laboratory
Lemont, Illinois 60439

Corresponding author: Thomas J. Phillips, Lawrence Livermore National Laboratory, Mail code L-103, Livermore, California 94550, email: phillips14@llnl.gov

Abstract

Several independent measurements of warm-season soil moisture and surface atmospheric variables recorded at the ARM Southern Great Plains (SGP) research facility are used to estimate the terrestrial component of land-atmosphere coupling (LAC) strength, and its regional uncertainty. The observations reveal substantial variation in coupling strength, as estimated from three soil moisture measurements at a single site, as well as across six other sites having varied soil and land cover types. The observational estimates then serve as references for evaluating SGP terrestrial coupling strength in the Community Atmospheric Model coupled to the Community Land Model. These coupled model components are operated in both a free-running mode and in a controlled configuration, where the atmospheric and land states are reinitialized daily, so that they do not drift very far from observations. Although the controlled simulation deviates less from the observed surface climate than its free-running counterpart, the terrestrial LAC in both configurations is much stronger, and displays less spatial variability, than the SGP observational estimates. Preliminary investigation of vegetation leaf area index (LAI) substituted for soil moisture suggests that the overly strong coupling between model soil moisture and surface atmospheric variables is associated with too much evaporation from bare ground, and too little from the vegetation cover. These results imply that model surface characteristics such as LAI, as well as the physical parameterizations involved in the coupling of the land and atmospheric components, are likely to be important sources of the problematical LAC behaviors.

1. Introduction

Land-atmosphere coupling (LAC) has important implications for weather and climate predictability, as well as the simulation of climatic change [Seneviratne et al., 2010; Orth and Seneviratne 2016]. The past fifteen years have witnessed numerous studies focusing on the coupling between soil moisture and diverse variables of the atmospheric boundary layer, as displayed by models, reanalyses, and observations.

Early LAC numerical experimentation utilized single models [Dirmeyer, 2001], but quickly advanced to execution of systematic intercomparison experiments involving multiple global climate models (GCMs) [Koster et al. 2002, 2004, 2006, 2010, 2011]. These GCM studies promoted the concept of "hot spots", located in semi-arid zones such as the U.S. Great Plains. Here the interactions of summertime soil moisture with surface temperature and humidity, and potentially also with precipitation mediated by local convection, are especially strong [Guo et al. 2006; Taylor et al., 2012; Gentine et al., 2013; Tawfik et al., 2015a, b]. In such moisture-limited regions--and especially in summer when radiative warming of the land is high--surface evaporation, humidity, and temperature are strongly influenced by soil moisture, and thus LAC tends to be most intense.

The GCM inter-comparisons inspired a subsequent wave of numerical experimentation focusing on details of LAC on different continents, which sometimes also employed mesoscale atmospheric models or regional climate models (RCMs) [e.g. Lawrence and Slingo, 2005; Seneviratne et al., 2006; Fischer et al., 2007; Meng and Quiring, 2010; Wei et al., 2010; Santanello et al., 2007, 2009, 2011b, 2013; Comer and Best, 2012, Dirmeyer et al. ,2012; Lorenz et al., 2012, 2015; Mei and Wang, 2012; Guo and Dirmeyer, 2013; Diro et al., 2014; Hirsch et al., 2014, 2016; Sun and Pritchard, 2016]. In addition, large-scale LAC was diagnosed in

multiple climate models participating in the Coupled Model Intercomparison Project (CMIP) [Notaro, 2008; Williams et al., 2012; Dirmeyer et al., 2013], which also included specialized experiments with prescribed versus prognostic soil moisture [Seneviratne et al., 2013; Berg et al., 2015]. More recently, modeling studies by Koster et al. [2016] and Zhou et al. [2016] highlighted remote interactions of soil moisture anomalies with the large-scale atmospheric circulation over North America.

As with free-running modeling experiments, reanalyses offer an opportunity to study LAC at continental to global scales, but with simulations that are steadily updated by assimilating available observations. Examples of this approach include work by Ruiz-Barradas and Nigam [2006], Luo et al. [2006], Wei and Dirmeyer [2010, 2012], Findell et al. [2011], Song et al. [2016], and Santanello et al. [2015]. In some instances also, LAC in several different reanalyses was compared with that in global or regional models [e.g. Zeng et al., 2010; Liu et al., 2014].

Unrealistic representations of LAC that are attributable to the models underlying the reanalyses [e.g. Santanello et al., 2015] have motivated alternative investigations using available observations. These include satellite-based investigation of large-scale LAC [Ferguson and Wood, 2011; Ferguson et al., 2012; Tuttle and Salvucci, 2016; Levine et al., 2016], local or regional-scale LAC estimated from *in situ* field observations [Kustas et al., 2005; Santanello et al., 2005; Dirmeyer et al., 2006; Lamb et al. ,2012; Ruiz Barradas and Nigam, 2013; Phillips and Klein, 2014; Guillod et al., 2014, 2015; Ford et al., 2015a, 2015b, 2017], or a mixture of both approaches [Miralles et al., 2012; Roundy and Santanello, 2017]. Many *in-situ* observational analyses have employed extensive data records suitable for LAC studies that are maintained by the U.S. Department of Energy Atmospheric Radiation Measurement (ARM) and AmeriFlux Programs [Mather . and Voyles, 2013; Hargrove et al. 2003]. In particular, the ARM Southern

Great Plains (SGP) facilities in Northern Oklahoma and Southern Kansas [Sisterson et al.,2016; Berg and Lamb, 2016] have provided the continuous data records required for investigations of LAC in a hot-spot region.

A few common themes run through results of the historical collection of modeling, reanalysis, and observational studies. One is that the coupling of soil moisture with surface atmospheric variables such as evaporation or temperature is generally more robust than its coupling with local precipitation via convective processes. Indeed, the extent to which soil moisture significantly impacts precipitation in different locations still remains unresolved, despite receiving much scientific attention [e.g. Findell et al., 2011; Taylor et al., 2012; Lamb et al., 2012; Ruiz-Barradas and Nigam, 2013; Phillips and Klein, 2014; Guillod et al., 2014, 2015; Ford et al. 2015a, 2015b, 2015c; Tuttle and Salvucci, 2016]. A conceptual framework for addressing the coupling of soil moisture with precipitation is to view this as a two-legged process: a *terrestrial* component involving soil moisture coupling with surface evaporation, and an *atmospheric* linkage between surface evaporation and convective precipitation [Guo et al., 2010; Dirmeyer, 2011; Santanello et al., 2011a; Tawfik et al., 2015a, 2015b]. Where model results have been compared with reanalyses or observations [e.g. Dirmeyer et al., 2006; Ruiz-Barradas and Nigam, 2006; Zeng et al., 2010; Ferguson et al., 2012; Phillips and Klein, 2014; Levine et al. , 2016], a second common theme is that simulatedcoupling of soil moisture with atmospheric variables is generally too strong, although this may depend on model-specific parameterizations [Lawrence and Slingo, 2005; Comer and Best, 2012; Mei and Wang, 2012; Sun and Pritchard, 2016].

Further investigation of the putative overly strong model representation of coupling strength motivates the present study, which focuses solely on the terrestrial link in the soil moisture-

136 atmospheric coupling chain. This focus ensures that a truly *local* estimate of the LAC strength is
137 obtained: if the atmospheric linkage were also to be investigated, effects on the 10-50 km
138 mesoscale would need to be taken into account.

139 Our study employs ARM *in situ* measurements in the SGP region to evaluate terrestrial LAC
140 in version 5.1 of the Community Atmospheric Model coupled to version 4 of the Community
141 Land Model [Neale et al., 2012; Oleson et al., 2010]. While the scarcity of *in situ* soil moisture
142 (SM) measurements often hinders reliable estimation of observed LAC, there exist three
143 independent data sets of shallow-depth SM, as well as alternative measurements of surface
144 atmospheric variables (e.g. latent/sensible heat fluxes, relative humidity, temperature) at the
145 Central Facility (CF) of the ARM Southern Great Plains site near Lamont, Oklahoma (at
146 coordinates 36.61 degrees North latitude and 97.48 degrees West longitude). In addition, there
147 are other SM and atmospheric measurements at ARM sites surrounding the CF that are sufficient
148 to allow estimation of terrestrial LAC in the SGP region. Of course, diverse measurements of
149 local soil moisture and surface atmospheric variables in the context of varying soil types and
150 vegetation covers are expected to give rise to different estimates of terrestrial LAC strength.
151 These strength differences provide a rough measure of the inherent uncertainties existing in
152 various aspects of the regional-scale LAC, and thus supply a reference standard for evaluating
153 similar LAC aspects simulated by the climate model.

154 Most previous modeling studies of LAC have employed simulations where both the
155 atmospheric and land components are initialized from model-specific climatologies, and where
156 soil moisture and temperature are spun-up until a quasi-equilibrium coupled climate state is
157 achieved. Subsequent numerical integration then usually proceeds with observed historical

158 variations in ocean sea surface temperatures (SSTs) and sea-ice extents prescribed, as in standard
159 Atmospheric Model Intercomparison Project (AMIP) experiments [Gates et al., 1999].
160 Our study also evaluates terrestrial LAC in such a free-running AMIP simulation of the
161 CAM5.1/CLM4 model. In addition, we make use of a continuous chain of CAM5.1 hindcasts in
162 which the atmospheric and land states are kept close to observations [Ma et al., 2015]. Running
163 the CAM5.1/CLM4 coupled system in such a controlled hindcast (HC) configuration has the
164 distinct advantage of mitigating biases introduced by the modeled atmospheric dynamics, in
165 order to highlight errors that are more closely tied to the model's parameterized physical
166 processes [Phillips et al., 2004]. Hence, a central focus of our study is to identify differences in
167 the strength and characteristics of land-atmosphere coupling that are displayed by the
168 CAM5.1/CLM4 when it is run in the free-running AMIP versus the controlled HC configuration.
169 The remainder of this paper is organized as follows. Section 2 describes the pertinent
170 measurements of soil moisture and surface atmospheric variables available at the SGP-CF site,
171 and . Section 3 includes discussion of the analysis approach and the metrics used for estimating
172 coupling strength, as well as the range of LAC results at both the CF site and over the broader
173 SGP region. In Section 4, the implementations of the free-running AMIP versus controlled HC
174 configurations of the coupled CAM5/CLM4 model are discussed. Their respective simulations of
175 terrestrial LAC are evaluated relative to the range of SGP observational estimates in Section 5,
176 and a general validation of surface variables in both the AMIP and HC simulations is conducted
177 at the SGP-CF site, where the requisite observations exist. assessed. Section 6 considers the use
178 of vegetation leaf area index (LAI) as an alternative coupling agent to that of soil moisture, and
179 discusses substantive differences between observed and modeled couplings with LAI at the SGP-
180 CF site. The simulated couplings with LAI also are used to interpret the contributions to local

surface evaporation of bare ground versus vegetated surfaces in the model. Finally, Section 7 offers concluding remarks.

2. Observational Data

Our study investigates LAC during the warm season (May-June-July-August or MJJA) when the land-atmosphere coupling at SGP is most intense. In the vicinity of the SGP-CF ungrazed pasture (grass-covered) site, three independent measurements of shallow-depth soil moisture (SM) are available for the years 2003-2011. These SM data sets are designated by the acronyms SWATS, EBBR, and CO2FLX, which may be accessed from the ARM Best Estimate-Land (ARMBELAND) section of the ARM data archive (http://www.archive.arm.gov/discovery) at hourly sampling intervals [Xie et al., 2014].

The Soil Water and Temperature System (SWATS) provides vertical profiles of soil temperature and moisture [Schneider et al., 2003; Bond, 2005]. The SWATS instrument imposes repeating electrical heating pulses, and measures the subsequent temperature rise and decay from heat dissipation. The lower the temperature rise and the more rapid its decay, the higher is the soil moisture content, with the exact relationship depending on the local soil texture and other properties. To provide measurement redundancy, SWATS observations are taken at multiple depths in 'east' and 'west' profiles spaced about a meter apart (designated as SWATS-E and SWATS-W). Where both profiles of data are available, these twin hourly SM values at the CF site were averaged, and treated as a single time series in our study. However, when data from one of these profiles suffer from extensive erroneous or missing values (e.g. for the west profile during the period MJJA of 2009-2011 at the CF site), only data from the alternative profile are used.

Co-located with the SWATS instrument at SGP-CF is the Energy Balance Bowen Ratio System (see fuller description below), whose chief purpose is to estimate surface latent and

sensible heat fluxes [Cook, 2016a]; but the EBBR instrumentation also includes an ancillary component that measures SM by five probes that detect the moisture-sensitive dielectric constant. The SM values are derived from an average of the readings over the five sensors and are reported in gravimetric units (kg water/kg soil) which are a function of local soil properties. From knowledge of the density of the local soil with respect to water, EBBR SM values are converted to the more commonly used volumetric units (m^3/m^3).

The Carbon Dioxide Flux Measurement Systems (CO2FLX) observations of soil moisture and various atmospheric variables are conducted near the center of a wheat field immediately south of the grass-covered CF site [Fischer, 2005]. Since wheat is typically harvested in June, during much of the MJJA study period this field is covered with either unharvested senescent wheat or wheat stubble that is equivalent to non-active vegetation. Hence, the CO2FLX observations are likely to display some deviations from those at the CF site that are due solely to differences in land cover. As in the EBBR SM instrumentation, CO2FLX SM sensors include electrodes and an oscillator whose resonant frequency depends on the dielectric constant (electrical capacitance) of the soil, which is sensitive to the moisture content.

EBBR measurements of SM are only made at 2.5-cm depth. CO2FLX observations are available at both 5-cm and 15-cm depths, and SWATS measurements range from depths of 5 cm to 175 cm at some ARM stations. For our study, however, only 5-cm depth values of CO2FLX and SWATS SM are considered, for comparison with the 2.5 cm EBBR measurements.

Figure 1 compares the temporal variation of these three estimates of shallow-depth soil moisture at the CF site, and in relation to observed precipitation events, during the MJJA season of the relatively dry and wet years 2006 and 2007, respectively. The SWATS SM data vary over a reduced range of values compared to both the CO2FLX and EBBR. This is especially evident

in the dry year 2006, when CO2FLX and EBBR valuesplunge to as low as about 0.1 m^3/m^3, while the minimum value of SWATS is only about 0.25 m^3/m^3. The anomalous minima of the SWATS SM data set result from the inability of its instrument probe to measure lower SM values than 0.25 m^3/m^3 [Cook and Kyrouac, 2015]. This is because the probe's electrical signal has difficulty penetrating soils with substantial clay content (as at the CF site) when soil moisture is low, making the calibration of the SWATS instrument problematic. (This limitation also exists for SWATS SM measurements made at lower depths at the CF site.)

On the other hand, there are substantially fewer missing values in the SWATS measurements than in the CO2FLX and EBBR SM data. Together with missing surface atmospheric observations, this substantially reduced the number of available soil moisture-atmospheric pairings to investigate. For a total of 1107 days in the MJJA 2003-2011 study period, for example, there were an average of 1076 daily soil moisture-atmospheric covariance pairs for SWATS, 875 for CO2FLX, and 822 for EBBR soil moisture measurements.

For our study, the available ARM atmospheric measurements of interest are surface air temperature T, relative humidity RH, and latent and sensible heat fluxes L and H. At the CF site, the ARM Best Estimate (ARMBE) archives were used as a primary source of data for these variables [Xie et al., 2010; Phillips and Klein, 2014], but alternative measurements also were used where available. For example, at the CF site the ARMBE surface temperature and humidity are measured by Surface Meteorological (SMET) probe transmitters [Ritsche, 2008], while alternative temperature and humidity measurements also are recorded by the CO2FLX instrument system [Fischer, 2005] that is located in the harvested wheat field just south of the CF site.

At the grass-covered CF site, the ARMBE surface turbulent fluxes are estimated by the EBBR instrumentation system [Cook, 2016a]. Flux estimates are derived from measurements of surface net radiation, ground heat flux, and the vertical gradients of temperature and relative humidity that are made by a net radiometer, temperature/relative humidity and soil temperature/moisture/heat flowprobes, and by a wind-speed sensor. The meteorological data are used to calculate bulk aerodynamic (BA) fluxes for producing a value-added product known as BAEBBR. This is a best-estimate of the turbulent fluxes that corrects sunrise/sunset spikes occurring in the raw EBBR fluxes, when the temperature and relative humidity gradients are of opposite sign and nearly equal in magnitude. The EBBR soil moisture at 2.5-cm depth also was used in order to calculate the soil heat conductivity, for correction of the soil heat flow plate measurements. Together with the temporal change in soil temperature measurements, this calculated conductivity provides an estimate of the ground heat flux, which impacts the magnitudes of the turbulent fluxes.

Eddy correlation (ECOR) sonic anemometers and H_2O/CO_2 analyzers provide alternative measurements of surface sensible and latent heat fluxes which are estimated directly from the correlation of vertical velocity with air temperature and water vapor density, respectively [Cook, 2016b]. Over the same surface, ECOR sensible and latent heat flux measurements are generally of smaller magnitude than those of the EBBR instrument, since the latter are forced to be equal to the local available energy. The ECOR instrument near SGP-CF is sited close to the boundary between the grass-covered CF site and the harvested wheat field to the south. ECOR measurements thus are influenced by both surface types (depending on wind direction), and so will also differ from the EBBR measurements on the grass-covered CF site. Another difference

272 is that the ECOR data near SGP-CF are available for one fewer warm season (MJJA of 2004-
273 2011) than the EBBR (MJJA of 2003-2011).

274 **3. Analysis Approach, Metrics, and Observational LAC Results**

275 To analyze the terrestrial component of LAC--whether in observations or model
276 simulations—we adopt the approach of Betts [2004, 2009], and focus on covariance relationships
277 between *daily averages* of soil moisture and surface atmospheric variables such as the turbulent
278 fluxes, relative humidity, and temperature. The daily average quantities are built up from hourly,
279 or in some cases half-hourly samples, while accounting for data gaps during the MJJA warm
280 seasons of 2003-2011 (see Phillips and Klein [2014] for details).

281 The covariance relationships are displayed as scatter plots, with daily averages of soil
282 moisture and of a specified atmospheric variable oriented along the x-axis and y-axis,
283 respectively. A quantitative measure of the coherence of an x-y scatter plot is provided by the
284 correlation coefficient R:

285 $$R = \mathrm{cov}(x,y)/ (\sigma_x\sigma_y) = \langle x'y' \rangle /(\sigma_x\sigma_y)$$

286 consisting of the temporal sum (denoted by < >) of the product of daily departures x' and y' of
287 each variable from its multi-year statistical mean value, where σ_x and σ_y are the corresponding
288 standard deviations. It may also be advisable to filter out the influence of the seasonal cycle (e.g.
289 by subtracting the multi-year climatology from each month's "raw data") before computing R.
290 However, other SGP studies of this type (Williams et al. [2015], Tang et al. [2017]) imply that
291 the impact of the seasonal cycle on LAC metrics is of second-order importance for this region.

292 Because R may be sensitive to mismatches in the standard deviations of the x and y
293 variables (i.e. large variability σ_y with small variability σ_x, or vice versa), Dirmeyer [2011]
294 recommends use of a "sensitivity index" I:

$$I = \sigma_x b$$

where $b = \mathrm{cov}(x,y)/\sigma_x^2$ is the slope of the least-squares regression line $y = a + bx$ calculated from the scatter of y versus x. Index I thus measures the magnitude of the average variation in y for a one-sigma variation in x, and takes on the same units as the y variable. It also can be seen that $I = \sigma_y R$, so that I and R are related through the scaling coefficient σ_y .We therefore employ I as an auxiliary LAC metric to R.

To assess the statistical significance of R, the number of statistically independent daily average samples of y versus x must be estimated. Accounting for data gaps, there are a minimum of about 822 x-y paired samples in the 2003-2011 MJJA records associated with the EBBR soil moisture data, which suffer the most data gaps; but because these samples are serially correlated, they are not all statistically independent. We attempted to estimate an upper bound for the serial correlation interval by analyzing the e-folding length of the autocorrelation function of the slowly varying SWATS data in seasons where data gaps were not an issue. From this limited analysis, we conservatively estimated that only every fifth daily average was statistically independent [see also Dirmeyer et al., 2012]. Under this assumption, the EBBR SM data set contains about 164 such samples. Applying a one-tailed Student's t test [e.g. Bulmer, 1979] that assumes physically based foreknowledge of the sign of the correlation indicates that $|R| > 0.18$ is statistically significant with probability $p = 0.01$ (i.e. a 99 percent confidence level). Where R is statistically significant, I is also assumed to be so, since it scales with R.

3.1 Observational Estimates of LAC at the SGP-CF site

The coupling between soil moisture and surface evaporation is central to the terrestrial component of LAC; but this coupling is better expressed by the covariance between SM and the evaporative fraction EF, which is a quasi-conserved quantity on daily time scales [Shuttleworth

et al.,1989; Gentine et al., 2011]. For measured values of surface latent heating L and sensible heating H,

$$EF = L/(L + H)$$

EF can be calculated from BAEBBR value-added estimates of L and H. Illustrative scatter plots of daily averages of EF with each of the independent shallow-depth SM measurements at CF (SWATS, CO2FLX, and EBBR) are shown in Figure 2. EF is seen to covary positively with all three SM measurements, and the LAC strength metric R ranges from a low value of 0.37 for the 2.5-cm-depth EBBR SM to a high value of 0.50 for the 5-cm-depth SWATS, with the 5-cm-depth CO2FLX SM measurements yielding an intermediate value of 0.39. The coupling metric I is similarly ordered, with a low value of .042 displayed by the EBBR SM, .053 by CO2FLX, and .065 by SWATS. (A corresponding disparity occurs when comparing LAC estimated from SWATS versus CO2FLX SM, both at 15-cm depths.)

Qualitatively similar covariance scatter is exhibited by the surface relative humidity RH (measured by the SMET system—see above description) versus the three SM measurements (Figure 3). The LAC metrics for RH also are ordered similarly to those for EF: the strongest coupling with RH is shown by SWATS SM (R = 0.55, I = 7.40%), and the weakest by EBBR (R = 0.37, I = 4.43%), with CO2FLX SM displaying intermediate coupling strength (R = 0.42, I = 5.75%).

In contrast to EF and RH, surface air temperature T (also measured by the SMET system) exhibits a negative covariation with soil moisture (Figure 4). The magnitude of LAC strength for SM-T coupling, as measured by the absolute value of the correlation coefficient R, is lower than for SM-EF or SM-RH couplings; but once again, the coupling of T with SWATS SM displays

the most negative magnitudes of R and I (-0.36 and -1.73 K, respectively), followed by CO2FLX (R = -0.32, I = -1.54 K) and EBBR SM (R = -0.27, I = -1.24 K).

The available 2003-2011 record length of warm-season observations was assumed sufficient for estimation of SM and LAC statistics of acceptable accuracy [Findell et al., 2015; Ford et al., 2016]. Analysis of the variations in R and I values for SM-EF coupling that occur with the progressive inclusion of each year's warm season (Table S1) raises some caveats, however. In general, the estimated values of R and I coupling metrics associated with the three independent SM measurements appear to "stabilize" after the inclusion of about seven warm seasons (2003-2009). However, including data for the last two years-- the very wet 2010 warm season and the very dry 2011--disrupts the relative stability of R and I attained for years 2003-2009, shifting their values by an average of several percent for correlations associated with SWATS SM, but by more than 10 percent for CO2FLX and EBBR SM. Thus, for nine years of warm-season measurements, the inclusion of data from a few exceptional years can alter the overall estimates of R and I to a surprisingly large degree for some SM measurements.

The consistently high LAC strength metrics for SWATS SM measurements, compared to those for CO2FLX or EBBR, also warrant further analysis. First, from comparison of Figures 2-4, the overall range of soil moisture values in daily average 5-cm SWATS data at SGP-CF is substantially less than what is found in either the CO2FLX or EBBR data. For instance, the minimum value of SWATS SM is about 0.25 m^3/m^3 (a consequence of the SWATS instrumental limitation mentioned in Section 2), which is much less dry than the lowest values seen in the other SM data sets thatlie below 0.1 m^3/m^3. It is therefore possible that the covariation of relatively low values of EF, RH, and T with an artificially high minimum SWATS SM may skew

362 the slopes of the respective regression lines higher, resulting in overestimation of the LAC
363 strength metrics.

364 We investigated the effects of imposing the same reduced range on the CO2FLX and EBBR
365 SM data when calculating their LAC metrics; but in following this protocol we found that R and
366 I for the non-SWATS data could not be raised substantially toward the corresponding higher
367 SWATS values. To cite one example: the covariation of T with EBBR SM restricted to values
368 greater than 0.25 m^3/m^3 yielded LAC strength metrics R = -0.30 and I = - 1.35.92 K, which are
369 only moderately different than the metrics obtained from the covariation of T with the
370 unrestricted EBBR SM (R = -0.27, I = -.1.24 K).

371 We also considered the possibility that the lower values of R and I metrics in the CO2FLX
372 data set might be explained by sampling errors in the CO2FLX or EBBR measurements, which
373 display many more data gaps than the SWATS. To test this hypothesis, the SWATS data were
374 degraded by eliminating daily average values of SM on those days where CO2FLX or EBBR
375 measurements showed missing data. Then the LAC strength metrics for the SM-EF, SM-RH, and
376 SM-T couplings were recalculated (see Table 1). While the EBBR-sampled SWATS data
377 produced LAC strength metrics R and I that were somewhat lower than the original SWATS data
378 set, the metrics calculated from the CO2FLX-sampled SWATS data were almost the same
379 magnitude. Variations in sample size among the three SM data sets thus are not sufficient to
380 explain the different magnitudes of the associated LAC strength metrics. These instead appear to
381 be due to differences in instrumentation, land cover, and depth of SM measurement.

382 The LAC metrics shown in Figures 2-4 reflect only differences in SM measurements. In
383 order to test the impacts of alternative measurements of the atmospheric variables on the LAC
384 metrics, latent and sensible heat fluxes recorded by the ECOR instrument (displaying the

385 influence of both grass-covered and wheat-covered surfaces) were substituted for the grass-
386 covered EBBR measurements. Observations of RH and T by the CO2FLX instruments on the
387 wheat-covered surface also were substituted for their SMET equivalents on the grass-covered CF
388 site. The impacts of these atmospheric-measurement substitutions on the LAC metrical values
389 are listed in Table 2, together with the R and I values shown in Figures 2-4. Only modest
390 differences in estimated LAC strengths (generally, more in I than in R) are seen to result from
391 such alternative atmospheric measurements, while the impacts of the different choices of SM
392 measurement are generally greater.

393 Of course, there is also an inherent statistical uncertainty in the estimated R value of an
394 atmospheric variable correlated with a particular soil moisture data set; but the probability
395 distribution of R becomes progressively more skewed as its sampled mean value increases,
396 making the estimation of confidence limits on R problematical. Instead, R can be transformed
397 into a normal variate Z:

398 $$Z = 0.5*\ln [(1+R)/(1-R)]$$

399 with standard error $\sigma_Z = 1/(n-3)^{1/2}$, where n is the number of statistically independent pairs of
400 soil versus atmospheric observations [Fisher, 1921]. The $+/-2\sigma_R$ (+/-95-percent) confidence
401 levels for R then can be obtained by an inverse transformation of the corresponding $Z +/- 2\sigma_Z$
402 values [e.g. Snedecor and Cochran, 1967]. (When R is negative, as for the SM-T correlation, the
403 absolute value of R is used to obtain Z, and the negative sign is restored after completing the
404 inverse transformation.)

405 Estimates of the range of the +/- 95-percent confidence limits for R values associated with
406 SWATS, CO2FLX, and EBBR soil moistures (assuming 215, 175, and 164 statistically
407 independent pairings, respectively) are listed in brackets in Table 1. The estimated +/- 95-percent

confidence intervals for each of the measured correlations R in Figures 2-4 are all found to overlap for the three different SM measurements, whether correlated with EF, RH, or T. For instance, in the case of SM-EF covariations (shown in Figure 2), the + 95-percent confidence limits for EF correlated with EBBR and CO2FLX soil moistures are 0.50 and 0.51, respectively, which exceed the -95-percent confidence limit of 0.39 for SWATS soil moisture (Table 1). Thus, from a purely statistical standpoint, correlations of the selected atmospheric variables with the three different soil moisture measurements cannot be distinguished from one another, at a 95-percent level of confidence.

3.2 Observational LAC estimated over the SGP region

Results reported in the last section imply substantial uncertainties in observed LAC strengths at the SGP-CF site. It should be possible to obtain a more statistically robust estimate of LAC by considering SM-EF covariation across the SGP region. Such a regionally representative estimate of LAC also should make a more suitable benchmark for evaluating coupling strength in CAM5.1/CLM4 model simulations that are realized on a 0.9 x 1.25-degree horizontal grid. This section illustrates how such a regionally aggregated estimate of SM-EF coupling strength, central to the terrestrial component of LAC, can be obtained.

While some two dozen ARM extended (E) facilities surround the CF site, there are only six where both soil moisture and atmospheric surface variables were recorded continuously over the MJJA 2003-2011 study period. Their geographic locations and soil/vegetation types are listed in Table 3. Available soil moisture observations at these E facilities include half hourly to hourly measurements of 2.5-cm EBBR and 5-cm SWATS soil moisture. Compared to the CF site, more SM data are missing for both the SWATS east and west soil profiles (SWATS-E and SWATS-W). Hence, instead of averaging profile values, it is necessary to choose SM values

from one or the other profile, depending on which includes the more complete data time series. However, an advantage of the SWATS soil moisture measurements at the E sites is that they extend over a moisture range comparable to that of the EBBR measurements, owing to soils that contain less clay than at the CF site (see Section 2.1 discussion and Table 3). At these E sites surface latent and sensible heat flux measurements, from which estimates of evaporative fraction EF can be derived, are provided by BAEBBR value-added products. On average, for the MJJA 2003-2011 study period, there are 740 SWATS SM-EF sample pairs at the selected E sites, and about 840 EBBR SM-EF pairs, yielding statistically independent sample sizes of about 148 versus 168, respectively.

In their detailed analysis of *in situ* observations of soil moisture over the conterminous U.S., Dirmeyer et al. [2016] found that the temporal variability of soil moisture was less sensitive to aggregation over neighboring sites than was the temporal mean. For estimating a regional average of SM-EF coupling strength, it thus seems advisable to spatially average a collection of locally calculated SM-EF values of R and I, rather than to compute these metrics from the scatter of SM and EF data that are spatially averaged. In fact, LAC metrics across the six E facilities display much spatial heterogeneity, exemplified by Figure S1 which contrasts SM-EF daily average scatter plots (employing both SWATS and EBBR SM versus EBBR EF data) at site E4 (Plevna, Kansas) and E12 (Pawhuska, Oklahoma). Despite quantitative differences in coupling estimates for SWATS versus EBBR SM, LAC strength metrics are consistently much higher at the E4 site (R = .55, I = .062 for SWATS; R = .50, I = .058 for EBBR SM) than at E12 (R= .09, I = .008 for SWATS; R = .14, I = .012 for EBBR SM), where the LAC strength metrics are so low that their statistical significance is questionable (see Section 2.2 discussion).

453 The range of SM values at site E4 (ranging between about 0.08 to .20 m^3/m^3 –Figure S1a
454 and S1b) versus those at E12 (ranging between about .21 to .40 m^3/m^3 –Figure S1c and S1d)
455 reflect a well-known west-east (eastward increasing) precipitation gradient across the SGP
456 region [Sisterson et al., 2016]. Because E4 experiences more moisture stress than E12, soil
457 moisture should generally exert greater control on warm-season EF at E4 [Phillips and Klein,
458 2014; Ford et al., 2015a; Nicholson, 2015], thus accounting for the observed stronger coupling at
459 E4. However, when considering the local LAC metrics across all six extended facility sites, such
460 an explanation seems too simplistic. For example, although average local soil moisture values at
461 sites E7, E9, E12, and E20 are all about 0.3 m^3/m^3, their LAC metrics differ substantially
462 (Table 3). This outcome implies that diverse local soil and land cover types (Table 3, column 2)
463 also strongly impact LAC strength across the SGP region. It suggests as well that the available
464 observations of shallow soil moisture are not very indicative of the impact that vegetation, rooted
465 at deeper soil depths, can have on EF.
466 Columns 5 and 6 of Table 3 list the SM-EF strength metrics R and I for SWATS versus
467 EBBR soil moisture, along with the range of estimated +/- 95-percent confidence levels. At each
468 site, the confidence intervals of SWATS-associated correlations overlap the EBBR-associated
469 ones, implying that the respective site-specific R values are statistically indistinguishable.
470 However, the very low SWATS- and EBBR-associated correlations at sites E9 and E12 can be
471 distinguished, with 95-percent confidence, from the highest correlations at sites E4 and E20. For
472 E9 this may be the result of the soil texture (loam), whereas for E12 it is likely influenced by the
473 vegetation (prairie tallgrass), whose roots extend to much greater depths than the pasture grass at
474 the other locations. Tallgrass plants draw most of their moisture from well below the 0-5cm top
475 layer of soil, and thus are less dependent than pasture grass on the shallow-layer SM.

Listed in the bottom row of Table 3 are the cross-site regional averages of R and I for SWATS (R = .35, I = .037) and EBBR (R = .31, I = .034) soil moistures, respectively, where these regional estimates are calculated from a simple linear averaging of R and I over the six E sites. In addition, an inverse-distance-weighting algorithm, centered on the CF site, is used to compute an alternative regional average of each LAC strength metric < M >:

$$< M > = \Sigma_i (w_i M_i) / \Sigma_i w_i \text{ , where weight } w_i = 1/ D_i$$

Here M_i is a strength metric R or I at an extended site E_i located at distance D_i from the CF site. D_i and the associated inverse-distance weights for each E site all are listed in Table 3. The corresponding weighted regional averages (i.e. summations of the weighted R and I values) are shown in parentheses at the bottom of columns 6 and 8 for SWATS (R = .31, I = .032) and EBBR (R=.27, I=.030), respectively. Weighted and unweighted regional average values of R and I thus do not differ much from one another, and they also are rather insensitive to the choice of SM data set: the regional-average R value lies between .27 and .35 (the corresponding I value between .030 and .037), which are indistinguishable with 95-percent confidence. These regional-average estimates of R and I provide observational benchmarks for evaluation of model simulations of SM-EF coupling strengths, to be taken up in following sections.

4. Model Properties and Simulation Configurations

The CAM5.1 atmospheric model [Neale et al., 2012] operates on a horizontal grid with resolution 0.9 x 1.25 degrees latitude/longitude and on a vertical grid of 30 levels. Its physical parameterizations include the radiative transfer scheme of Iacono et al. [2008], shallow and deep convective parameterizations after Park and Bretherton [2009], Zhang and McFarlane [1995], and Neale et al. [2008], a planetary boundary layer and associated moist turbulence scheme developed by Bretherton and Park [2009], prognostic cloud physics and microphysics schemes

499 of Morrison and Gettelman [2008], Gettelman et al. [2010], and Park et al. [2014], and a
500 prognostic aerosol scheme after Liu et al. [2012].
501 The CLM4 land model [Oleson et al., 2010] uses the same horizontal grid as the
502 atmospheric model, includes 15 vertical soil layers and 5 snow layers, and accounts for
503 heterogeneity in surface types (glacier, lake, wetland, etc.). The CLM4 represents vegetated
504 surfaces by as many as 16 plant functional types (PFTs). In our simulations, a version of CLM4
505 *without* dynamic vegetation or carbon fluxes was employed, and distinct vegetation properties
506 such as PFT fractions and canopy top and bottom heights instead were prescribed for each
507 gridbox. Leaf and stem area indices (LAI and SAI) were similarly prescribed, but varied
508 temporally according to monthly climatologies.
509 Surface radiative fluxes account for vegetation and canopy properties, and turbulent fluxes
510 follow Monin-Obukhov similarity theory, as formulated by Zeng et al. [1998]. Depth-dependent
511 moisture storage in CLM4 is the net outcome of parameterized precipitation infiltration, surface
512 and sub-surface runoff, diffusion of soil water, sub-column drainage, and interactions with
513 groundwater, as described by Zeng and Decker [2009].
514 We investigated simulations in which the CAM5.1/CLM4 coupled system was run in two
515 qualitatively different configurations: free-running Atmospheric Model Intercomparison Project
516 (AMIP) and controlled hindcast (HC) simulations, both over the period 1997 to 2012. In the
517 AMIP simulation, observed sea surface temperatures (SSTs) and sea ice extents (SIEs) were
518 prescribed as ocean boundary conditions. The atmospheric and land states both were initialized
519 from a model climatology determined after a prior long spin-up of soil moisture. For the
520 controlled HC configuration, the SSTs and SIEs also were prescribed as in the AMIP
521 experiment, but the three-dimensional fields of atmospheric prognostic dynamic and

thermodynamic state variables instead were initialized at the beginning of each simulation day according to their ERA-Interim Reanalysis values. Initialization of prognostic aerosol concentrations proceeded by nudging the atmospheric U and V winds, using a Newtonian relaxation method, toward their ERA-Interim values. (Nudging only the model winds resulted in more realistic aerosol concentrations than when the model atmospheric temperature and humidity were also nudged toward ERA-Interim values.) The daily initial conditions for the land state were determined by running the CLM4 in an offline configuration, where it was forced with observed winds, precipitation, and downward shortwave and longwave surface radiative fluxes. This land initialization procedure yielded more realistic values of soil moisture than in the free-running AMIP simulation.

For each day's initialization of atmosphere and land, hindcasts (i.e. model forecasts of historical weather conditions) were generated over the following three days, with a steadily increasing drift of the model hindcasts from observations. Since day-1 hindcasts often show spurious perturbations resulting from initialization "shock", LAC results for day-2 hindcasts were analyzed in our study (see Ma et al. [2015] for further details).

5. Evaluation of Model LAC: Free-Running versus Controlled Configurations

Similarities and differences in LAC displayed by the model in its free-running AMIP versus controlled HC configurations, as well as comparisons with the observed estimates of LAC at both the CF site and across the SGP region, are discussed next.

51 Model evaluation near the SGP-CF site

In this section, all reported model results are those simulated at the grid point (with coordinates 36.28 N, 97.50 W) that lies nearest to the SGP-CF site (at 36.61 N, 97.48 W). Scatter plots of the covariances of coupled CAM5.1/CLM4 daily averages of EF, RH, and T with respect

545 to 5-cm depth soil moisture are shown in Figure 5 for the AMIP simulation. LAC strength
546 metrics R and I for the respective AMIP-simulated couplings are seen to lie well above the
547 highest observational LAC estimates at the CF site, which are associated with the SWATS soil
548 moisture measurements (Figures 2-4). The model exceedance of the observed strength metrics is
549 especially dramatic for the SM-T coupling, where AMIP values R = -.80 and I = -4.45 K are more
550 than twice as large as the highest SM-T observational estimates (R = -.36, I = -1.73 K, Figure 4).
551 Figure 6 shows the corresponding scatter plots for the controlled HC simulation. The scatter
552 of EF versus SM (Figure 6a) displays a "kink" at an SM value of about 0.3 m^3/m^3, which is
553 somewhat more pronounced than in the AMIP simulation (Figure 5a). Further investigation of
554 the scatter of EF associated with evaporation from bare ground versus vegetated fractions of this
555 model grid cell imply that this feature results from an abrupt leveling off in the variation of bare-
556 ground EF for SM values greater than about 0.3 m^3/m^3. The clear signature of bare-ground
557 evaporation in Figure 6a suggests that it is a strong contributor to the total EF in this model grid
558 cell. As is found for the AMIP simulation (Figure 5), the LAC strength metrics for HC lie well above
559 the highest observational estimates associated with the SWATS soil moisture data (Figures 2-4).
560 The SM-EF and SM-RH coupling strengths for the HC simulation are slightly less than those for
561 the AMIP run (compare Figures 5a/6a and 5b/6b), but the SM-T coupling strength for the HC is
562 markedly less (R = -.53, I = -2.50 K) than that for AMIP (R = -.80, I = -4.5 K).
563 The very tight SM-T coupling in the AMIP simulation relative that for the HC (Figures
564 5c/6c) apparently results from the free-running model's more frequent "visits" to drier soil
565 moisture states than in the controlled HC simulation. For instance, we can identify the "dry"
566 portion of the model's SM-EF transition zone (between completely wilted and fully saturated
567 SM conditions) with SM values less than ~0.25 m^3/m^3, and the "wet" portion with SM values

568 greater than ~ 0.35 m^3/m^3. Then about 64 percent of SM values for the AMIP configuration are
569 found to occur at "dry" levels, while only about 6 percent rise to "wet" levels; for the controlled
570 HC configuration, however, the dry/wet SM frequencies are instead 34 and 19 percent,
571 respectively.

572 When soil moisture in semi-arid regions such as the SGP falls into drier states, its coupling
573 with surface atmospheric variables tends to increase [Phillips and Klein, 2014; Ford et al., 2015a;
574 Nicholson, 2015]. Meanwhile, surface EF falls, while surface sensible heat flux H and
575 temperature T rise. The enhanced SM-T coupling for drier SM states in the free-running AMIP
576 configuration tends to amplify a continental warm bias that is present in simulations of the
577 CAM5.1/CLM4, as well as in many other current-generation GCMs [e.g. Klein et al., 2006;
578 Cheruy et al., 2014; Van Weverberg et al., 2015; Merrifield and Xie, 2016; and Morcrette et al.,
579 2017, Van Weverberg et al. 2017, Ma et al. 2017, and Zhang et al., 2017--in review]. In the
580 controlled HC configuration, however, soil moisture is prevented from falling as frequently into
581 drier states because the land model is initialized each day by forcing it with observed
582 precipitation. Hence, the SM-T coupling is less intense in the HC simulation than in the free-
583 running AMIP.

584 Figure 7 compares time series of daily average precipitation rate P near the CF site in both
585 AMIP and HC simulations with CF-observed values in the MJJA warm season of the relatively
586 dry/wet years 2006/2007. Observed MJJA precipitation is seen to occur in sharp spikes with
587 maximum amplitude about 80 mm day^{-1}; but precipitation events in the AMIP simulation remain
588 mostly below 10 mm day^{-1} intensity. As would be expected in a free-running simulation of this
589 type, the modeled precipitation also does not align well with the timing of the observed events.
590 There is a better correspondence of the timing of modeled and observed P events in the HC

591 simulation (a consequence of its more realistic atmospheric and land states); but the simulated
592 amplitudes remain mostly too low: although the HC soil moisture is more realistically initialized
593 each day, it still "feels" the effects of the too-scant model precipitation amounts on *intra-diurnal*
594 time scales.

595 While under-predicting precipitation peaks in the observed time series, the accumulated
596 seasonal precipitation in both the AMIP and HC simulations (Figure S3) configurations
597 moderately exceed the observations during the dry 2006 warm season. This disparity appears to
598 result from a pervasive "drizzle effect" (Stephens et al. [2010]), wherein climate models are
599 found to rain out in smaller amounts and at higher frequencies than are observed. In the much
600 wetter 2007 warm season, however, both configurations show pronounced shortfalls in
601 accumulated precipitation (in the AMIP run, more than in the HC).

602 Table 4 summarizes the LAC metrics for the AMIP and HC simulations, and compares these
603 with observational values that are linearly averaged over the three SM data sets listed in Table 1.
604 For each LAC metric, the +/- 95-percent confidence intervals also are shown in brackets, where
605 it is assumed that the observational averages constitute 164 statistically independent daily soil
606 moisture-atmospheric pairs (the same as that associated with the EBBR SM measurements,
607 which suffered the most missing data). Because there are no missing model data, the
608 corresponding number of statistically independent samples are 221 (every fifth day in a total of
609 1107 in MJJA 2003-2011). The AMIP and HC R metrics are all much higher than the
610 corresponding observational averages, and also are distinguishable with 95-percent confidence
611 from the latter. In contrast, when comparing the AMIP versus HC correlations, only the SM-T
612 couplings are clearly distinguishable. This suggests that the AMIP-HC differences in SM-T
613 coupling strength may not only be a consequence of the HC's more realistic land state, but also

may depend on AMIP-HC differences in radiative and hydrological forcings of the land, as well as parameterizations that govern the latent and sensible heat transfers at the soil-atmosphere interface.

Listed in Table 5 are model performance statistics (mean bias, root-mean-square error RMSE, and modeled versus observational temporal variance ratio σ_m^2/σ_o^2) of AMIP- and HC-simulated single variables at the near-CF grid point, evaluated relative to ARMBE observations at the CF site. All performance metrics are computed using daily average model and observational values for the 2003-2011 MJJA warm seasons. The evaluated model variables include forcings of the land surface (precipitation, net surface shortwave and longwave radiative fluxes) and of land response variables (surface latent and sensible heat fluxes, evaporative fraction, surface relative humidity and temperature, and soil moisture at 5-cm depth).

From Table 5, the precipitation rate is negatively biased in both simulations, but is less so in the controlled HC configuration, as Figure 7 implies. In both simulations also, the modeled net surface shortwave heating is under-predicted, while the surface net longwave cooling is over-predicted, resulting in an excessive overall radiative cooling of the surface. The controlled HC run shows a lesser radiative cold bias than the AMIP, however.

The surface latent heat flux is negatively biased for both model configurations, while the surface sensible heat flux is biased positive for the AMIP, but negative for the HC. These turbulent flux differences yield an evaporative fraction that is smaller than observed for the AMIP run, but larger than observed for the HC. Both model configurations display negatively biased surface relative humidity (consistent with underpredicted latent heat fluxes) and positively biased surface air temperature (consistent with overpredicted net upward longwave radiation).

636 Hence, the modeled atmospheric surface layer is systematically too warm and dry, although
637 much more so in the AMIP run than in the HC.
638 Simulated soil moisture is a model-specific variable [Koster et al., 2009], and so will not
639 necessarily agree closely with observations. For example, the modeled SM at 5-cm depth for
640 both the AMIP and HC simulations is closer to that of the SWATS measurements, which at the
641 CF site do not display as large a range of variation as the CO2FLX data. (The 5-cm soil moisture
642 performance statistics are not calculated relative to EBBR measurements at 2.5 cm depth.) The
643 tendency of the free-running AMIP simulation to frequent drier soil moisture states than that of
644 the HC results in a substantially lower mean value of SM (0.234 versus 0.281 m^3/m^3).
645 It is not surprising that RMS errors listed in Table 5 are generally less for the controlled HC
646 configuration than for the free-running AMIP, which cannot be expected to closely reproduce the
647 observed day-to-day variations. Temporal variance ratios σ_m^2/σ_o^2 also are usually more realistic
648 for the HC simulation than for AMIP. The modeled soil moisture variance at CF is similar to that
649 of the CO2FLX observations, but is more than twice as high as that for the SWATS
650 observations. (The latter disparity probably can be discounted, since the variability of the
651 SWATS measurements seems anomalously low at the CF site--see Figures 2-4.) However, for
652 several other variables, the modeled variability is either decidedly too large (surface net
653 longwave flux, evaporative fraction, relative humidity) or too small (precipitation rate, surface
654 net shortwave flux, surface turbulent fluxes).
655 From the standpoint of the representation of land-atmosphere coupling, the model's
656 underprediction of both precipitation amplitude and frequency is perhaps the most troubling.
657 These forcing errors impact the soil moisture, the humidity of the boundary layer, and the
658 turbulent fluxes—all key elements for determining LAC strength.

659 **5.2 Model LAC evaluated at regional scale**

660 The LAC strengths of the model in both AMIP and HC configurations at the near-CF grid
661 point are significantly larger than the observational estimates. However, this grid point
662 "represents" a gridbox of dimension 0.9 x 1.25-degrees, and so there is a danger of a scale
663 mismatch in such a single-point comparison with observations. A fuller evaluation of the
664 CAM5.1/CLM4 model thus demands examination of its simulation of LAC across the SGP
665 region. Here, we compare the SM-EF coupling, central to the terrestrial component of LAC,
666 against the observational estimates of this quantity that are discussed in Section 2.3.2.

667 Besides the near-CF model grid point (at 36.28 N, 97.50 W), eleven grid boxes span the
668 3 x 3-degree latitude/longitude SGP region. In both AMIP and HC simulations also, the MJJA
669 climatological precipitation displays only a weak spatial gradient that is oppositely directed
670 (westward increasing) to that of the observations (eastward increasing). The model-prescribed
671 regional soil types have varying percentages of sand and clay, and the prescribed vegetation
672 cover mostly consists of generic grass and crop plant functional types [Oleson et al., 2010].
673 These prescribed quantities probably are unlikely to fully capture the observed spatial inter-site
674 variations in surface characteristics that are listed in Table 3.

675 Scatter plots of SM-EF covariances for both AMIP and HC simulations at a grid box that is
676 northwest of the near-CF grid point, and for one to its east, are shown in Figure S2. Because
677 these locations roughly correspond to those of the E4 and E12 observational stations, these
678 model plots can be compared with the observed results shown in Figure S1. The model LAC
679 metrics near the E12 location (Figures S2c and S2d) are much greater than those observed at the
680 E12 station (Figures S1c and S1d). Moreover, the observed *differences* in LAC metrics between

681 the E4 and 12 stations (Figures S1a versus S1c, and S1b versus S1dd) are absent in the modeled
682 representations (Figures S2a versus S2c, and S2b versus S2d).

683 SM-EF strength metrics R and I for the free-running AMIP simulation are provided across
684 eleven model grid boxes in Table S2, and for the controlled HC simulation in Table S3. In the
685 AMIP run (Table S2), there is little variation in the R and I values across model grid boxes, in
686 contrast to their pronounced spatial heterogeneity in region-wide observations (Table 3). For the
687 HC simulation (Table S3), there is somewhat more cross-grid heterogeneity, with R values
688 ranging between .49 to .74 and I values between .050 to .14. Presumably, this is mostly a
689 consequence of the controls that keep the HC atmospheric and land states more realistic than
690 those in the free-running AMIP simulation.

691 Both distance-weighted and unweighted regional averages of R and I values are listed in the
692 bottom rows of Tables S2 and S3, along with an estimate of +/- 95-percent confidence intervals,
693 given in brackets. These metrics display little sensitivity to whether a weighted or unweighted
694 averaging procedure is followed. They also are very similar for the AMIP (R = .65, I = .11-.12)
695 versus the HC (R = .66-.67, I = .10) model configurations. The metrical values all substantially
696 exceed the corresponding observational regional averages (R = .27 to .35, I = .030 to.037) listed
697 in the bottom row of Table 3, and they are statistically distinguishable (with 95-percent
698 confidence) from the observational averages. Thus, the hypothesis that the modeled SM-EF
699 coupling strengths of the CAM5.1/CLM4 model are too high across the SGP region is confirmed
700 with 95% confidence.

701 **6. Vegetation as an Alternative Coupling Agent**

702 Except over bare-ground areas, the coupling of soil moisture with the surface atmosphere is
703 mediated by vegetation, where the ratio of the local area of the vegetation relative to that of bare

ground is commonly expressed by a non-dimensional leaf area index (LAI). Williams and Torn [2015] estimated LAI at the grass-covered CF site, and at the adjacent wheat field where the CO2FLX instruments are located. They inferred LAI from the normalized difference vegetation index (NDVI) calculated from visible and near-infrared reflectances measured by radiometers at both locations. Williams and Torn [2015] also showed that during daylight hours (when the respective land covers are photosynthetically active, the coupling between LAI and the evaporative fraction EF is markedly stronger than that between 10 cm-depth SWATS soil moisture and EF. This is because plant roots tap into soil moisture at greater depths than is immediately available in bare-ground locations, and the evaporative flux associated with transpiration is strongly regulated by vegetation stomatal conductance (proportional to LAI). The mediating vegetation thus plays a larger role in LAC coupling than does the shallow-depth soil moisture at these SGP locations--a result that is also in accord with the regional modeling study of Hirsch et al. [2014] over Australia.Because the version of CLM4 used in our study does not include dynamic vegetation. Instead, LAI (inferred from satellite measurements of phenology), is prescribed as a seasonal-cycle climatology. However, this model prescription does not account forthe substantial inter-annual/intra-seasonalvariability in LAI that accompanies differences in precipitation amounts and timings during individual warm seasons (see Figure 8).Although the 2003-2011 MJJA mean values of observed versus modeled LAI are of roughly comparable magnitudes (observed mean = 1.88, model mean = 1.14), their inter-annual/intra-seasonal variabilities are very different.

The consequences of these stark differences in LAI variability are illustrated by Figure 9, which contrasts the scatter plot of daylight (hours 12 Z to 23 Z) averages of EF versus LAI that are observed at the CF site with those simulated by the CAM5.1/CLM4 model at the closest grid

point to the CF site. The diminished coherence of the LAI-EF interaction in the model relative to the observational estimate (reflected by much lower model R and I metrics) is striking. However, if the observations of LAI are restricted to the same range as that of the model (LAI values between 0.9 and 1.4—see Figure 8b), the observational LAC strength metrics of Figure 8a are reduced to R = 0.27 and I = 0.030--of the same order as the simulated values R = 0.18 and I = 0.029. The model's underestimation of local LAI-EF coupling strength thus seems to be mostly a consequence of the CLM4 prescription of LAI with greatly reduced inter-annual/intra-seasonal range, which does not include observed changes in LAI that depend on the relatively wet or dry character of a particular MJJA warm season (Figure 9).

Using only point observational estimates of LAI in Figures 8a and 9 is, admittedly, not an ideal standard for evaluating the modeled LAI-EF coupling, since a grid-point value of LAI represents a spatial average of several different types of land cover that occupy the associated grid box. The estimation of *in-situ* LAI from NDVI requires measurements of spectrally-resolved albedo, which are only available currently at the CF site. A fairer *in-situ* test of the modeled LAI-EF coupling at regional scale thus awaits future measurements of spectral reflectance at ARM extended facility sites. Nevertheless, judicious interpretation of Figures 8 and 9 suggests that 1) LAI is an essential complement to shallow-depth soil moisture for estimating terrestrial land-atmosphere coupling strength, and 2) realistic inclusion of the inter-annual/intra-seasonal variability of LAI in models is important for accurately representing this coupling strength [see also Ford and Quiring, 2013 and Zscheischler et al., 2015].

Recent work by Tang et al. [2017] seems to corroborate these assertions. Estimating the regional LAI-EF coupling strength from SGP-downscaled satellite observations of LAI and from EBBR in-situ measurements of EF for 2004-2011 warm seasons, Tang et al. show that the

750 strength of the LAI-EF coupling exceeds that of the corresponding shallow-depth SM-EF
751 coupling at six out of eight sites in the SGP region.

752 Considering the model LAC results of Section 3, and taking the implications of Figures 8
753 and 9 at face value, the CAM5.1/CLM4 appears to overestimate the SM-EF coupling, while
754 underestimating LAI-EF coupling near the CF site. As previously mentioned in our discussion of
755 Figure 6a, these results suggest that more modeled surface evaporation emanates from the bare-
756 ground fraction of the near-CF grid cell than from the vegetated fraction. Figure 10, showing
757 MJJA time series of the model's surface evaporation from bare ground versus vegetation in
758 specific wet and dry years, appears to confirm this hypothesis.

759 Williams et al. [2016] also found a similar disproportion in the SM-EF versus LAI-EF
760 coupling strengths occurring in a single-column version of the NCAR Community Earth System
761 Model (CESM1.2.2) atmosphere, when centered on the SGP-CF site and coupled to the CLM4.5
762 land model [Oleson, Lawrence et al. 2013]. In attempting to correct these coupling biases,
763 Williams et al. [2016] modified selected properties of the CLM4.5 model: they prescribed model
764 LAI according to the observational estimates of Williams and Torn [2015], while also increasing
765 bare-soil resistance to evaporation, the minimum moisture conductance of vegetation stomata,
766 and leaf reflectance. These modifications improved the single-column model predictions for the
767 warm seasons at the CF site, especially during the dry 2006 summer, when large negative biases
768 in precipitation and positive biases in surface temperature were greatly reduced. Williams et al.
769 [2016] also performed offline CLM4.5 simulations at the CF site, where inputs of the Williams
770 and Torn [2015] LAI estimates were included separately from the modified model physics
771 parameterizations. They found that the LAI and physics changes were approximately of equal

772 importance as potential explanations for the discrepancies between modeled and observed
773 terrestrial coupling metrics.

774 The performance improvements for the offline CLM and single-column atmospheric model
775 offer some hope for reducing excessive model LAC through physically based alterations of land
776 surface/vegetation characteristics. Of course, implementing similar changes in a more complex
777 climate model such as the coupled CAM5.1/CLM4 may well prove to be a more difficult
778 undertaking [e.g. Hirsch et al., 2016].

779 **7. Concluding Remarks**

780 Our study investigates the terrestrial component of observed land-atmosphere coupling
781 (LAC) at local and regional scales on the U.S. Southern Great Plains (SGP), and its
782 corresponding representation in the CAM5.1/CLM4 coupled atmospheric/land model, when
783 configured in both free-running Atmospheric Model Intercomparison Project (AMIP) and
784 controlled hindcast (HC) simulations.

785 The main points of this study can be summarized as follows:

786 • Different measurements of shallow-depth soil moisture SM reveal considerable
787 variability in observational estimates of LAC and its spatial variability across the
788 SGP region;

789 • The spatial variability in observed LAC appears to be associated with an intra-
790 regional gradient in the moisture climatology, but also to local variations in soil type
791 and land cover;

792 • The coupling of surface evaporative fraction with vegetation leaf area index (LAI) is
793 substantially stronger than that with shallow-depth SM, presumably because LAI

794 serves as a proxy for root-level soil moisture and plant physiological characteristics
795 that mediate the interaction between soil moisture and surface evapotranspiration;
796 • When the CAM5.1/CLM4 model is run in the HC configuration, the biases in
797 simulated forcings and state variables are generally reduced, in comparison with
798 those in the free-running AMIP configuration;
799 • To some extent, these HC-AMIP forcing differences act to shift the LAC behaviors
800 of the model, but in both model configurations the SM-EF coupling strength is much
801 greater than the observational estimates, while it displays substantially less spatial
802 variability across the region;
803 • In contrast, the coupling of LAI with EF in the model seems too weak at a site where
804 this can be estimated observationally, and may be due to an under-specification of
805 LAI inter-annual/intra-seasonal variability and/or to under-representation of surface
806 evaporation from the vegetated fraction of the model grid box.

807 In the discussion that follows, we elaborate on these salient points.

808 For our study, three alternative choices of Atmospheric Radiation Measurement (ARM) soil
809 moisture observations were available at the SGP-CF site, each having different strengths and
810 weaknesses, were available. An inherent limitation was that only the coupling of atmospheric
811 surface variables with soil moisture at shallow depths (2.5-5.0 cm) could be compared. In future
812 investigations of this type, it would be preferable to estimate observed LAC strengths over a
813 range of depths spanning the vegetation rooting. Hence, it is noteworthy that a successor ARM
814 Soil Temperature and Moisture Profile (STAMP) system measuring soil moisture over five
815 depths at some seventeen SGP extended facilities has been deployed since 2015 [Cook, 2016c].

816 Even for shallow soil depths, considerable uncertainty is evident in observed estimates of
817 LAC strength based on the three different observations of shallow soil moisture. This uncertainty
818 is greatest at the CF site, where artifacts in the reported SWATS soil moisture characteristics
819 make these data markedly different from those of the CO2FLX and EBBR. At each of six ARM
820 extended regional facilities surrounding the CF site, lesser differences in estimated SM-EF LAC
821 strength using SWATS and EBBR soil moistures are found than at the CF site. Spatial variations
822 in LAC strength across the SGP region are substantial, however, due partly to differences in soil
823 wetness that reflect an observed west-east precipitation gradient across the region; but diverse
824 local soil and land cover types also appear to strongly influence observed regional spatial
825 variability in LAC strength.
826 With its more realistic atmosphere/land initialization, the controlled HC configuration
827 ameliorates the excessive deviations of the AMIP simulation from SGP-CF observations, but
828 sizeable biases still remain. (The comparison of gridbox values to point-wise observations at the
829 CF site introduces some ambiguity in the evaluation of the model performance, however.) The
830 HC simulation's over-prediction of variability in evaporative fraction EF and surface relative
831 humidity RH, despite its under-prediction of variability in precipitation and surface radiation,
832 implies that the model's excessive terrestrial LAC will not be corrected solely by improving
833 these model forcings. It appears that the detailed physics of the model's interactions among soil
834 moisture, the surface turbulent fluxes, and the surface temperature and humidity states also will
835 need to be improved. The model representation of LAC strength in both the AMIP and HC
836 simulations nonetheless clearly lies outside the envelope of observational uncertainty across the
837 SGP region. Model prediction of overly strong LAC can have significant consequences on a

range of time scales: overestimation of the influence of the land on the atmospheric state is likely to produce erroneous weather forecasts, seasonal predictions, and climate-change projections.

Another clue as to a possible cause of the deficient representation of LAC by the CAM5.1/CLM4 is provided by considering vegetation LAI as an alternative coupling agent to soil moisture. Compared to the observational evidence (limited to the CF site), the apparently too-weak coupling of EF with LAI, and its too-strong coupling with soil moisture, suggests that the overly strong representation of LAC may be related to the simulation of evaporation from bare ground areas, in excess of that from the vegetation cover. Thus, model surface characteristics such as LAI and evaporation resistance parameters, in addition to physical parameterizations of surface fluxes, may also be responsible for the problematic simulation of LAC.

Before CAM/CLM developers can begin to improve the modeled representation of LAC, they will require a more precise, process-oriented diagnosis of the detailed physics of soil moisture and vegetation interactions with surface fluxes and temperature/moisture states. Because of the continual correction of the coupled atmosphere/land state that is implemented in the HC configuration of the model, this simulation lends itself to such a process-oriented investigation. For example, if high-frequency atmospheric observations are available, it is feasible to evaluate *daily* model hindcasts, or composites of such hindcasts organized according to synoptic type (e.g. dry- versus wet-day behaviors). Such a fine-grained analysis contrasts with the strictly statistical evaluation of free-running climate simulations that is typically employed. Planned future work therefore will exploit these advantages of the HC model configuration.

We anticipate that LAC studies at different spatiotemporal scales will become increasingly feasible with the advent of soil-moisture sensing satellites such as SMOS (Soil Moisture Ocean

Salinity, Kerr et al. [2010]) and SMAP (Soil Moisture Active Passive, Entekhabi et al. [2010]), as well as growing networks of *in-situ* data such as ISMN (International Soil Moisture Network, Dorigo et al. [2011]), NASMD (North American Soil Moisture Database, Quiring et al. [2016]), SCAN (Soil Climate Analysis Network, Strobel et al. [2016], www.wcc.nrcs.usda.gov/scan), and the fledgling NSMN (National Soil Moisture Network, Strobel et al. [2016]). Given that so little is known about the detailed physics of LAC, other studies that pursue diverse diagnostic approaches, and that apply these to different types of models, are to be strongly encouraged.

Acknowledgments

We acknowledge the U.S. Department of Energy (DOE) Atmospheric Radiation Measurement (ARM) program for funding the recording of CO2FLX, EBBR, and SWATS soil moisture and the ARMBE and other atmospheric data sets. The SGP observational data sets used in this study can all be accessed from the ARM archives via the Data Discovery interface at http://www.archive.arm.gov/discovery. Model data used in this study will be made available via a file transfer protocol (ftp) upon request. The work of TJP, SAK, YM, QT, and SX was funded by the U.S. Department of Energy Office of Science under its ARM, Atmospheric System Research (ASR), and Regional and Global Modeling (RGCM) programs, and was performed at the Lawrence Livermore National Laboratory under Contract DE-AC52 07NA27344. INW and MST were supported by the U.S. Department of Energy Atmospheric System Research under contract DE-AC02-05CH11231. The work of DRC was funded by the U.S. Department of Energy Office of Science Under its ARM Program, and was performed at Argonne National Laboratory under contract DE-AC02-06CH11357.

References

Berg, L.K., and P.J. Lamb (2016), Surface properties and interactions: Coupling the land and atmosphere within the ARM program, in *The Atmospheric Radiation Measurement (ARM) Program: First 20 Years, Meteorological Monographs, Vol. 57,* American Meteorological Society, Boston, Massachusetts.

Berg, A., B. Lintner, K. Findell, S. Seneviratne, B.van den Hurk, F. Cheruy, A. Ducharne, S. Hagemann, D. Lawrence, S. Malyshev, A. Meier, and P. Gentine (2015), Interannual coupling between summertime surface temperature and precipitation over land: Processes and implications for climate change, *J. Climate, 28*, 1308–1328.

Betts, A.K. (2004), Understanding hydrometeorology using global models, *Bull. Amer. Meteor. Soc*., *85*, 1673-1688.

Betts, A.K. (2009), Understanding land-surface-atmosphere coupling in observations and models, *J. Adv. Modeling Earth Systems*, *1*, 18 pp., doi:10.3894/JAMES.2009.1.4.

Bond, D. (2005), Soil water and temperature system (SWATS) handbook, ARM Technical Report TR-063, 24 pp., U.S. Department of Energy, Washington, D.C.,

Bretherton, C.S., and S. Park (2009), A new moist turbulence parameterization in the Community Atmosphere Model. *J. Climate*, *22*, 3422-3448.

Bulmer, M.G. (1979), *Principles of Statistics*, 252 pp., Dover Publications Inc., New York.

Cheruy, F., J.L. Dufresne, F. Hourdin, and A. Ducharne (2014), Role of clouds and land-atmosphere coupling in midlatitude continental summer warm biases and climate change amplification in CMIP5 simulations, *Geophys. Res. Lett*., *41*, 6493-6500.

Comer, R.E., and M.J. Best (2012), Revisiting GLACE: Understanding the role of the land surface in land-atmosphere coupling, *J. Hydrometeor*., *13*, 1704-1718.

Cook, D.R. (2016a), Energy balance Bowen ratio (EBBR) handbook, ARM Tech. Rept. DOE/SC-ARM/TR-037, 24 pp., US Department of Energy Office of Science, Washington, D.C.

Cook, D.R., 2016b: Eddy correlation flux measurement system instrument handbook, ARM Tech. Rept. DOE/SC-ARM/TR-052, 18 pp., US Department of Energy Office of Science, Washington, D.C.

Cook, D.R., 2016c: Soil temperature and moisture profile (STAMP) system handbook. ARM Tech. Rept. DOE/SC-ARM-TR-186, 24 pp., US Department of Energy Office of Science, Washington, D.C.

Cook, D.R., and J. Kyrouac (2015), SWATS present and future, presented at the Sixth ARM/ASR Joint User Facility and Principal Investigator Meeting, Vienna, Virginia, March 16 – 20.

Dirmeyer, P.A. (2001), An evaluation of the strength of land-atmosphere coupling, *J. Hydrometeor*., *2*, 329-344.

Dirmeyer, P.A. (2011), The terrestrial segment of soil moisture-climate coupling. *Geophys. Res. Lett., 38*, L16702, doi:10.1029/2011GL048268.

936 Dirmeyer, P.A., R.D. Koster, and Z. Guo (2006), Do global models properly represent the
937 feedback between land and atmosphere?, *J. Hydrometeor*., *7*, 1177-1198, DOI: 10.1175/
938 JHM532.1.

939 Dirmeyer, P.A. et al. (2012), Evidence for enhanced land-atmosphere feedback in a warming
940 climate, *J. Hydrometeor*,*13*, 981-995.

941 Dirmeyer, P.A., Y. Jin, B. Singh, and X. Yan (2013), Evolving land-atmosphere interactions
942 over North America from CMIP5 simulations, *J. Climate*, *26*, 7313-7326.

943 Dirmeyer, P.A., J. Wu, H.E. Norton, W.A. Dorigo, S.M. Quiring, T.W. Ford, J.A.
944 Santanello, M.G. Bosilovich, M.B. Ek, R.D. Koster, G. Balsamo, and D.M. Lawrence
945 (2016), Confronting weather and climate models with observational data from soil
946 moisture networks over the United States, *J. Hydrometeor.*, *17*, 1049-1067.

947 Diro, G.T., L. Sushama, A. Martynov, D.I. Jeong, D. Verseghy, and K. Winger (2014),
948 Land-atmosphere coupling over North America in CRCM5, *J. Geophys. Res*., *119*,
949 doi:10.1002/2014D021677.

950 Dorigo, W.A. et al. (2011), The International Soil Moisture Network: A data hosting facility
951 for global in situ soil moisture measurements, *Hydrol. Earth Syst. Sci*., *15*, 1675-1698.

952 Entekhabi, D., et al. (2010), The Soil Moisture Active Passive mission, *Proc. IEEE*, *98*, 704-
953 716.

954 Ferguson, C.R., and E.F. Wood, (2011), Observed land-atmosphere coupling from satellite
955 remote sensing and reanalysis. *J. Hydrometeor*., *12*, 1221-1254.

956 Ferguson, C. R., E. F. Wood, and R. K. Vinukollu (2012), A global intercomparison of
957 modeled and observed land-atmosphere coupling, *J. Hydrometeor*., *13*, 749-784.

958 Findell, K.L., P. Gentine, B.R. Lintner, and C. Kerr (2011), Probability of afternoon
959 precipitation in eastern United States and Mexico enhanced by high evaporation, *Nature*
960 *Geosci.*, doi:10.1038/ ngeo1174.

961 Findell, K.L., P. Gentine, B.R. Lintner, and B. P. Guillod (2015), Data length requirements
962 for observational estimates of land-atmosphere coupling strength, *J. Hydrometeor., 16*,
963 1615-1635.

964 Fischer, M.L. (2005), Carbon dioxide flux measurement systems, ARM Technical Report
965 TR-048, 11 pp., U.S. Department of Energy Office of Science, Washington, D.C.

966 Fisher, R.A. (1921), On the "probable error" of a coefficient of correlation deduced from a
967 small sample, *Metron*, *1*, 1-3.

968 Fischer, E.M., S.I. Seneviratne, D. Luthi, and C. Schar (2007), Contribution of land-
969 atmosphere coupling to recent European summer heat waves, *Geophys. Res. Lett*., *34*,
970 L06707, doi:10.1029/2006GL029068.

971 Ford, T.W., and S.M. Quiring (2013), Influence of MODIS-derived dynamic vegetation on
972 VIC-simulated soil moisture in Oklahoma, *J. Hydrometeor*, *14*, 1910-1921.

973 Ford, T.W., A.D. Rapp, S.M. Quiring, and J. Blake (2015a), Soil-moisture-precipitation
974 coupling: observations from the Oklahoma Mesonet and underlying physical
975 mechanisms, *Hydrol. Earth Syst. Sci.*, *19*, 3617-3631.

Ford, T.W., A.D. Rapp, and S.M. Quiring (2015b), Does afternoon precipitation occur preferentially over dry or wet soils in Oklahoma?, *J. Hydrometeor*., *16*, 874-888.

Ford, T.W., S.M. Quiring, O.W. Frauenfeld, and A.D. Rapp (2015c), Synoptic conditions related to soil moisture-atmosphere interactions and unorganized convection in Oklahoma, *J. Geophys. Res.*, *120*, doi:10.1002/2015JD023975.

Ford, T., Q. Wang, and S. Quiring (2016), The observation record length necessary to generate robust soil moisture percentiles, *J. Appl. Meteor. Climatol*., doi:10.1175/ JAMC-D-16-0143.

Ford, T.W., S.M. Quiring, and O.W. Frauenfeld (2017), Multi-decadal variability of soil moisture-temperature coupling over the contiguous United States modulated by Pacific and Atlantic sea surface temperatures, *Int. J. Climatol*., *37*, 1400-1415.

Gates, W.L. et al. (1999), An overview of the results of the Atmospheric Model Intercomparison Project (AMIP1), *Bull. Amer. Meteor. Soc*., *80*, 29-55.

Gentine, P., D. Entekhabi, and J. Polcher (2011), The diurnal behavior of evaporative fraction in the soil-vegetation-atmospheric boundary layer continuum. *J. Hydrometeor.*, *12*, 1530-1546.

Gentine, P., A.A.M. Holtslag, F. D'Andrea, and M. Ek (2013), Surface and atmospheric controls on the onset of moist convection over land, *J. Hydrometeor*., *14*, 1443-1462.

Gettelman, A., A. X. Liu, S. J. Ghan, H. Morrison, S. Park, A. J. Conley, S. A. Klein, J. Boyle, D. L. Mitchell, and J. L. F. Li (2010), Global simulations of ice nucleation and ice supersaturation with an improved cloud scheme in the community atmosphere model, *J. Geophys. Res*., *115*, D18216, doi:10.1029/2009JD013797.

Guillod, B.P., et al. (2014), Land-surface controls on afternoon precipitation diagnosed from observational data: uncertainties and confounding factors, *Atmos. Chem. Phys*., *14*, 8343-8367.

Guillod, B.P., B. Orlowsky, D.G. Miralles, A.J. Teuling, and S.I. Seneviratne (2015), Reconciling spatial and temporal soil moisture effects on afternoon precipitation, *Nat. Commun*., *6*, 6443.

Guo, Z. et al. (2006), The Global Land-Atmosphere Coupling Experiment. Part II: Analysis. *J. Hydrometeor*., *7*, 611-625.Guo, Z., and P.A. Dirmeyer (2013), Interannual variability of land-atmosphere coupling strength, *J. Hydrometeor*., *14*, 1636-1646.

Hargrove, W.W., F.M. Hoffman, and B.E. Law (2003), New analysis reveals representativeness of the AmeriFlux network, Eos, Transactions American Geophysical Union, 84(48), pp. 555.

Hirsch, A.L., A.J. Pitman, and J. Kala (2014), The role of land cover change in modulating the soil moisture-temperature land-atmosphere coupling strength over Australia, *Geophys. Res. Lett*., *41*, 5883-5890.

Hirsch, A.L., A.J. Pitman, and V. Haverd (2016), Evaluating land-atmosphere coupling using a resistance pathway framework, *J. Hydrometeor*., *17*, 2615-2630.

Iacono, M., J. Delamere, E. Mlawer, M. Shephard, S. Clough, and W. Collins (2008), Radiative forcing by long-lived greenhouse gases: Calculations with the AER radiative transfer models, *J. Geophys. Res.*,*113*, D13103, doi: doi:10.1029/2008JD009944.

1015 Kerr, Y. et al. (2010), The SMOS mission: New tool for monitoring key, *Proc. IEEE, 98*,
1016 666-687.

1017 Klein, S., X. Jiang, J. Boyle, S. Malyshev, and S. Xie (2006), Diagnosis of the summertime
1018 warm and dry bias over the U.S. Southern Great Plains in the GFDL climate model
1019 using a weather forecasting approach, *Geophys. Res. Lett.*, *33*, L18805,
1020 doi:10.1029/2006GL027567.

1021 Koster, R.D., P.A. Dirmeyer, A.N. Hahmann, R. Ijpelaar, L.Tyahla, P. Cox, and M.J.
1022 Suarez, (2002), Comparing the degree of land-atmosphere interactions in four
1023 atmospheric general circulation models, *J. Hydrometeor*., *3*, 363-375.

1024 Koster, R.D. et al. (2004), Regions of strong coupling between soil moisture and
1025 precipitation, *Science, 305*, 1138-1140.

1026 Koster, R.D. et al. (2006), GLACE: The Global Land-Atmosphere Coupling Experiment.
1027 Part I: Overview *J. Hydrometeor*., *7*, 590-610.

1028 Koster, R.D., Z. Guo, R. Yang, P.A. Dirmeyer, K. Mitchell, and M.J. Puma (2009), On the
1029 nature of soil moisture in land surface models, *J. Climate, 22*, 4322-4335.

1030 Koster, R.D. et al. (2010), Contribution of land surface initialization to subseasonal forecast
1031 skill: First results from a multi-model experiment, *Geophys. Res. Lett.*, *37*, L02402,
1032 doi:10.1029/2009GL041677.

1033 Koster, R.D. et al. (2011), The second phase of the global land-atmosphere coupling
1034 experiment: Soil moisture contributions to subseasonal forecast skill, *J. Hydrometeor*.,
1035 *12*, 805-822.

1036 Koster, R.D., Y. Chang, H. Wang, and S.D. Schubert (2016), Impacts of local soil moisture
1037 anomalies on the atmospheric circulation and on remote surface meteorological fields
1038 during boreal summer: A comprehensive analysis over North America, *J. Climate*, *29*,
1039 7345-7364.

1040 Kustas, K.P., J.L. Hatfield, and J.H. Prueger (2005), The soil moisture-atmosphere coupling
1041 experiment (SMACEX): Background, hydrometeorological conditions, and preliminary
1042 findings. *J. Hydrometeor*., *6*, 791-804.

1043 Lamb, P.J., D.H. Portis, and A. Zangvil (2012), Investigation of large-scale atmospheric
1044 moisture budget and land surface interactions over U.S. Southern Great Plains including
1045 for CLASIC (June 2007), *J. Hydrometeor.*, *13*, 1719-1738.

1046 Lawrence, D.M., and J. M. Slingo (2005), Weak land-atmosphere coupling strength in
1047 HadAM3: The role of soil moisture variability, *J. Hydrometeor., 6*, 670-680.

1048 Levine, P.A., J.T. Randerson, S.C. Swenson, and D.M. Lawrence (2016), Evaluating the
1049 strength of the land-atmosphere feedback in Earth system models using satellite
1050 observations, *Hydrol. Earth Syst. Sci*., *20*, 4837-4856.

1051 Liu, X. et al. (2012), Toward a minimal representation of aerosols in climate models:
1052 Description and evaluation in the Community Atmosphere Model CAM5, *Geosci.*
1053 *Model Dev.*, *5***,** 709-739.

Liu, D., G. Wang, R. Mei, Z. Yu, and H. Gu (2014), Diagnosing the strength of land-atmosphere coupling at subseasonal to seasonal time scales in Asia, *J. Hydrometeor*., *15*, 320-339.

Lorenz, R., E.L. Davin, and S.I. Seneviratne (2012), Modeling land-climate coupling in Europe: Impact of land surface representation on climate variability and extremes, *J. Geophys. Res*., *117*, doi:10.1029//2012D017755.

Lorenz, R., A.J. Pitman, A.L. Hirsch, and J. Srbinovsky (2015), Intraseasonal versus interannual measures of land-atmosphere coupling strength in a global climate model: GLACE-1 versus GLACE-CMIP5 experiments in ACCESS1.3b, *J. Hydrometeor*., *16*, 2276-2295.

Luo, Y., E.H. Berbery, K.E. Mitchell, and A.K. Betts (2006), Relationships between land surface and near-surface atmospheric variables in the NCEP North American Regional Reanalysis, *J. Hydrometeor*., *8*, 1184-1203.

Ma, H-Y., C. C. Chuang, S. A. Klein, M.-H. Lo, Y. Zhang, S. Xie, X. Zheng, P.-L. Ma, Y. Zhang, and T. J. Phillips (2015), Evaluation and diagnosis of physical processes in GCMs with an improved hindcast approach: Experiments with specified SST and sea ice, *J. Adv. Mod. Earth Sys*., *7*, 1810-1827.

Ma H.-Y et al. (2017), CAUSES: On the role of surface energy budget errors to the warm surface air temperature over the Central U.S., *J. Geophys. Res.* (in research).

Mather, J.H., and J.W. Voyles (2013), The ARM Climate Research Facility: A review of structure and capabilities. *Bull. Amer. Meteor. Soc*., *94*, 377-392.

Mei, R., and G. Wang (2012), Summer land-atmosphere coupling strength in the United States: Comparison among observations, reanalysis data, and numerical models, *J. Hydrometeor*., *13*, 1010-1022.

Meng, L., and S.M. Quiring (2010), Examining the influence of spring soil moisture anomalies on summer precipitation in the U.S. Great Plains using the Community Atmosphere Model version 3, *J. Geophys. Res*., *115*, D21118, doi:10.1029/ 2010JD014449.

Merrifield, A.L., and S-P. Xie (2016), Summer U.S. surface air temperature variability: Controlling factors and AMIP simulation biases, *J. Climate, 29*, 5123-5139.

Miralles, D.G., M.J. van den Berg, A.J. Teuling, and R.A.M. de Jeu (2012), Soil moisture-temperature coupling: A multiscale observational analysis. *Geophys. Res. Letters*, *39*, L21707, doi:10.1029/2012GL053703.

Morcrette, C. et al. (2017), the Clouds Above the United States and Errors at the Surface (CAUSES) project. Part 1: Near-surface temperature errors in numerical weather prediction and climate model 5-day hindcasts near the Southern Great Plains, *J. Geophys. Res*. (in review).

Morrison, H., and A. Gettelman (2008), A new two-moment bulk stratiform cloud microphysics scheme in the NCAR Community Atmosphere Model (CAM3), Part I: Description and numerical tests, *J. Climate, 21*, 3642-3659.

Neale, R. B., J. H. Richter, and M. Jochum (2008), The impact of convection on ENSO: From a delayed oscillator to a series of events, *J. Climate*, *21*, 5904–5924.

Neale, R.B et al. (2012), Description of the NCAR Community Atmosphere Model (CAM5.0), NCAR Technical Note NCAR/TN-486+STR, 274 pp., National Center for Atmospheric Research, Boulder, Colorado.

Nicholson, S.E. (2015), Evolution and current state of our understanding of the role played in the climate system by land surface processes in semi-arid regions, *Global and Planet. Change*, *133*, 201-222.

Notaro, M. (2008), Statistical identification of global hot spots in soil moisture feedbacks among IPCC AR4 models, *J. Geophys. Res*., *113*, D09101, doi:10.1029/2007JD009199.

Oleson, K. W. et al. (2010), Technical description of version 4.0 of the Community Land Model (CLM), NCAR Technical Note, NCAR/TN-478+STR, 266 pp., National Center for Atmospheric Research, Boulder, Colorado

Oleson, K.W., D. M. Lawrence, et al. (2013), Technical description of version 4.5 of the Community Land Model (CLM), NCAR Technical Note, NCAR/TN-503+STR, 434 pp., National Center for Atmospheric Research, Boulder, Colorado.

Orth, R., and S. Seneviratne (2016), Variability of soil moisture and sea surface temperatures similarly important for warm-season land climate in the Community Earth System Model, *J. Climate*, doi: 10.1175/JCLI-D-15-0567.1

Park, S., and C.S. Bretherton (2009), The University of Washington shallow convection and moisture turbulence schemes and their impact on climate simulations with the Community Atmosphere Model, *J. Climate*, *22*, 3449-3469.

Park, S., C.S. Bretherton, and P.J. Rasch (2014), Integrating cloud processes in the Community Atmosphere Model, Version 5, *J. Climate*, *27*, 6821-6856.

Phillips, T.J., and S.A. Klein (2014), Land-atmosphere coupling manifested in warm-season observations on the U.S. Southern Great Plains, *J. Geophys. Res*., *119*, 509-528.

Phillips, T.J. et al. (2004), Evaluating parameterizations in general circulation models: Climate simulation meets weather prediction, *Bull. Amer. Meteor. Soc*., *85*, 1903-1915.

Quiring, S.M., T.W. Ford, J.K. Wang, A. Khong, E. Harris, T. Lindgren, D.W. Goldberg, and Z. Li (2016), The North American soil moisture database, *Bull. Amer. Meteor. Soc.*, *97*, 1441-1459.

Ritsche, M.T. (2008), Surface meteorological observation system handbook, ARM Tech. Rept. DOE/SC-ARM TR-031, 31 pp., U.S. Department of Energy Office of Science, Washington D.C.

Roundy, J.K., and J.A. Santanello (2017), Utility of satellite sensing for land-atmosphere coupling and drought metrics, *J. Hydrometeor*., *18*, 863-877.

Ruiz-Barradas, A., and S. Nigam (2006), Great Plains hydroclimatic variability: The view from the North American Regional Reanalysis, *J. Climate*, *19*, 3004-3010.

Ruiz-Barradas, A., and S. Nigam (2013), Atmosphere-land surface interactions over the Southern Great Plains: Characterization from Pentad Analysis of DOE ARM field observations and NARR, *J. Climate*, *26*, 875-886.

Santanello, J.A., M. Friedly, and W.P. Kustas (2005), An empirical investigation of convective planetary boundary layer evolution and its relationship with the land surface, *J. Appl. Meteor*., *44*, 917-932.

Santanello, J.A., M.A. Friedl, and M.B. Ek (2007), Convective boundary layer interactions with the land surface at diurnal time scales: Diagnostics and feedbacks, *J. Hydrometeor*., *8*, 1082-1097

Santanello, J.A., C.D. Peters-Lidard, S.V. Kumar, C. Alonge, and W.-K. Tao (2009), A modeling and observational framework for diagnosing local land-atmosphere coupling on diurnal time scales. *J. Hydrometeor*., *10*, 577-599.

Santanello, J.A., C. Ferguson, M. Ek, P. Dirmeyer, O. Tuinenburg, C. Jacobs, C. van Heerwaarden, K. Findell, P. Gentine, and B. Lintner (2011a), Local land-atmosphere coupling (LoCo) research: Status and results, pp. 7-9 in *GEWEX News*, *Vol. 21*, No. 4.

Santanello, J.A., C. D. Peters-Lidard, and S.V. Kumar (2011b), Diagnosing the sensitivity of local land-atmosphere coupling via the soil moisture-boundary layer interaction, *J. Hydrometeor*., *12*, 766-786.

Santanello, J.A., C.D. Peters-Lidard, A. Kennedy, and S.V. Kumar (2013), Diagnosing the nature of land-atmosphere coupling: A case study of dry/wet extremes in the U.S. Southern Great Plains, *J. Hydrometeor*., *14*, 3-24.

Santanello, J.A., J. Roundy, and P.A. Dirmeyer (2015), Quantifying the land-atmosphere coupling behavior in modern reanalysis products over the U.S. Southern Great Plains, *J. Climate, 28*, 5813-5829.

Schneider, J.M., D.K. Fisher, R.L. Elliott, G.O. Brown, and C.P. Bahrmann (2003), Spatio-temporal variation in soil water: First results from the ARM SGP CART Network, *J. Hydrometeor*., *4*, 106-120.

Seneviratne, S.I., D. Luthi, M. Litschi, and C. Schar (2006), Land-atmosphere coupling and climate change in Europe, *Nature*, *443*, 205-209.

Seneviratne, S.I., T. Corti, E.L. Davin, M. Hirschi, E.B. Jaeger, I. Lehner, B. Orlowsky, and A.J. Teuling (2010), Investigating soil moisture-climate interactions in a changing climate: A review, *Earth Sci. Rev*., *99*, 125-161.

Seneviratne, S.I., et al. (2013), Impact of soil moisture-climate feedbacks on CMIP5 projections: First results from the GLACE-CMIP5 experiment, *Geophys. Res. Lett.*, *40*, 5212-5217.

Shuttleworth, W.J., R.J. Gurney, A.Y. Hsu, J.P. Ormsby (1989), FIFE: The variation in energy partition at surface flux sites. *IAHS Publ*., *186*, 67-74.

Sisterson, D.L., R.A. Peppler, T.S. Cress, P.J. Lamb, and D.D. Turner (2016), The ARM Southern Great Plains (SGP) site in The Atmospheric Radiation Measurement (ARM) Program: First 20 Years, *Meteorological Monographs, Vol. 57*, American Meteorological Society, Boston, Massachusetts.

Snedecor, G.W., and W.G. Cochran (1967), *Statistical Methods*, 6th ed., 593 pp., Iowa State University Press, Ames, Iowa..

Song, H-J., C.R. Ferguson, and J.K. Roundy (2016), Land-atmosphere coupling at the Southern Great Plains Atmospheric Radiation Measurement (ARM) field site and its role in anomalous afternoon peak precipitation, *J. Hydrometeor*., *17*, 541-556.

Stevens, G.L, et al. (2010), Dreary state of precipitation in global models, *J. Geophys. Res*., *115*, D24211, doi: 10.1029/2010JD014532.

Strobel, M., J. Lucido, S. Quiring, C. McNutt, and V. Deheza (2016), Building a coordinated national soil moisture monitoring network, presented at the National Soil Moisture Network Workshop, U.S. Department of Agriculture Natural Resources Conservation Service, Boulder, Colorado, 24-26 May.

Sun, J. and M.S. Pritchard (2016), Effects of explicit convection on global land-atmosphere coupling in the super-parameterized CAM, *J. Adv. Model. Earth Syst*., *8*, 1-22.

Tang, Q., S. Xie, Y. Zhang, T.J. Phillips, J.A. Santanello, D.R. Cook, L. Riihimaki, and K. Gaustad (2017), A new metric for land-atmosphere coupling strength: Application to ARM observations over the U.S. Southern Great Plains, *J. Geophys. Res*. (in review).

Tawfik, A.B., P.A. Dirmeyer, and J.A. Santanello (2015a), The heated condensation framework. Part I: Description and Southern Great Plains case study. *J. Hydrometeor*., *16*, 1929-1945.

Tawfik, A.B., P.A. Dirmeyer, and J.A. Santanello (2015b), The heated condensation framework. Part II: Climatological behavior of convective initiation and land-atmosphere coupling over the conterminous United States, *J. Hydrometeor*., *16*, 1946-1961.

Taylor, C.M., R.A.M. de Jeu, F. Guichard, P.P. Harris, and W.A. Dorigo (2012), Afternoon rain more likely over drier soils, *Nature*, *489*, 423-426.

Tuttle, S., and G. Salvucci (2016), Empirical evidence of contrasting soil moisture-precipitation feedbacks across the United States, *Science*, *352*, 825-828.

Van Weverberg, K., Morcrette, C. J., Ma, H.-Y., Klein, S. A. and Petch, J. C. (2015), Using regime analysis to identify the contribution of clouds to surface temperature errors in weather and climate models, *Q.J.R. Meteorol. Soc*., *141*. 3190–3206.

Van Weverberg et al. (2017), Attribution of surface radiation errors near the Southern Great Plains in numerical weather prediction and climate models, *J. Geophys. Res*. (in review).

Wei, J., and P.A.Dirmeyer (2010), Toward understanding the large-scale land-atmosphere coupling in the models: Roles of different processes, *Geophys. Res. Lett*., *37*, L19707, doi:10.1029/ 2010GL044769.

Wei, J., P.A. Dirmeyer, and Z. Guo (2010), How much do different land models matter for climate simulation? Part II: A decomposed view of land-atmosphere coupling strength, *J. Climate*, *23*, 3135-3145.

Wei, J., and P. Dirmeyer (2012), Dissecting soil moisture-precipitation coupling, *Geophys. Res. Lett.*, *39*, L19711, doi:10.1029/2012GL053038.

Williams, C.J.R., R.P. Allan, and D.R. Kniveton (2012), Diagnosing atmosphere-land feedbacks in CMIP5 climate models, *Environ. Res. Lett.*, *7*, doi:10.1088/1748-9326/4/044003.

Williams, I.N., and M.S. Torn (2015), Vegetation controls on surface heat flux partitioning, and land-atmosphere coupling, *Geophys. Res. Lett.*, *42*, 9416-9424.

Williams, I.N., Y. Lu, L.M. Kueppers, and W.J. Riley (2016), Land-atmosphere coupling and climate prediction over the U.S. Southern Great Plains, *J. Geophys. Res.*, *121*, 12125-12144.

Xie, S.C., et al. (2010), ARM Climate Modeling Best Estimate Data: A new product for climate studies, *Bull. Amer. Meteor. Soc.*, *91*, 13-20.

Xie, S.C., et al. (2014), ARM Best Estimate (ARMBELAND) Southern Great Plains Central Facility (C1) dataset, http://www.arm.gov/data/eval/78, Atmospheric Radiation Measurement (ARM) Climate Research Facility Data Archive.

Zeng, X., Zhao, M., and Dickinson, R.E. (1998), Intercomparison of bulk aerodynamic algorithms for the computation of sea surface fluxes using the TOGA COARE and TAO data, *J. Climate*, *11*, 2628-2644.

Zeng, X., and Decker, M. (2009), Improving the numerical solution of soil moisture-based Richards equation for land models with a deep or shallow water table, *J. Hydrometeor.* *10*, 308-319.

Zeng, X., M. Barlage, C. Castro, and K. Fling (2010), Comparison of land-precipitation coupling strength using observations and models, *J. Hydrometeor.*, *11*, 979-994.

Zhang, C. et al. (2017), CAUSES: Diagnosis of the summertime warm bias in CMIP5 models at the ARM Southern Great Plains site, *J. Geophys. Res*. (in review).

Zhang, G. J., and N. A. McFarlane (1995), Sensitivity of climate simulations to the parameterization of cumulus convection in the Canadian Climate Centre general circulation model, *Atmosphere-Ocean*, *33***,** 407–446.

Zhou, Y., D. Wu, W.K.-M. Lau, and W-K. Tao (2016), Scale dependence of land-atmosphere interactions in wet and dry regions as simulated with NU-WRF over the Southwestern and South-Central United States, *J. Hydrometeor.*, *17*, 2121-2136.

Zscheischler, J., R. Orth, and S.I. Seneviratne (2015), A submonthly database for detecting changes in vegetation-atmosphere coupling, *Geophys. Res. Lett.*, *42*, doi:10.1002/2015GL06656

Table 1: For the SGP-CF site, correlation R and sensitivity index I of the atmospheric surface evaporative fraction EF(estimated from BAEBBR measurements of the turbulent fluxes), relative humidity RH, and air temperature T, with respect to the SWATS SM data. Rand I values also are shown for SWATS data that are reduced according to available CO2FLX and EBBR soil moisture samples for the MJJA warm seasons in 2003-2011. Also listed are the R and I values of EF, RH, and T associated with the CO2FLX and the EBBR soil moisture data. The most extreme positive or negative value of the correlation for each atmospheric variable is shown in red, and the least extreme value in blue. In addition, the range of +/- 95-percent confidence levels for the R values associated with the SWATS, CO2FLX, and EBBR soil moisture measurements are shown in brackets (assuming 215, 175, and 164 statistically independent pairs of atmospheric and soil moisture variables, respectively--see Section 3.1 discussion).

Soil Moisture measurement	EF	RH	T
SWATS	R = .50 [.39 to .60] I = .065	R = .55 [.45 to .64] I = 7.40 %	R = - .36 [-.24 to -.47] I = -1.73 K
CO2FLX-sampled SWATS	R = .52 I = .070	R = .54 I = 7.32 %	R = -.38 I = - 1.82 K
EBBR-sampled SWATS	R = .42 I = .049	R = .47 I = 5.52 %	R = - .22 I = - 1.00 K
CO2FLX	R = 0.39 [.25 to .51] I = .053	R = 0.42 [.29 to .54] I = 5.75 %	R = -0.32 [-.18 to -.45] I = -1.54 K
EBBR	R = 0.37 [.23 to .50] I = .042	R = 0.37 [.23 to .50] I = 4.43 %	R = -0.27 [-.12 to -.41] I = -1.24 K

Table 2: 2003-2011warm-season (MJJA) correlations R and sensitivity coefficients I of the SWATS, EBBR, and CO2FLX shallow-depth soil moisture content measurements with respect to observationally based estimates of surface evaporative fraction EF, and surface relative humidity RH and temperature T, all in the vicinity of the SGP-CF site (coordinates 36.61 N, 97.48 W). Here, EF is derived from surface latent and sensible heat fluxes that are measured by the BAEBBR system, or alternatively, by the ECOR instrument which is part of the CO2FLX system located in a wheat-covered field adjacent to the CF site. The RH and T values are ARM Best Estimate (ARMBE) data obtained from the ARM Surface Meteorology Observation System (SMET) instruments or from CO2FLX tower measurements. Note that the ECOR data are available only for the years 2004-2011, while all others are for the period 2003-2011.

Soil Moisture Data Sets	EF		RH		T_s	
	BAEBBR	ECOR	SMET	CO2FLX	SMET	CO2FLX
SWATS	R = .50 I = .065	R = .54 I = .083	R =.55 I = 7.40 %	R = .51 I = 6.52 %	R = -.36 I = -1.73 K	R = -.37 I = -1.80 K
CO2FLX	R = .39 I = .053	R = .40 I = .061	R =.42 I =5.75 %	R = .44 I = 5.58 %	R = -.32 I = -1.54 K	R = -.30 I = -1.46 K
EBBR	R = .37 I = .042	R = .47 I = .064	R = .37 I = 4.43 %	R = .38 I = 4.43 %	R = -.27 I = -1.24 K	R = -.26 I = -1.19 K

Table 3: Selected extended facility geographical location, dominant soil and vegetation types**,** and distance from the CF. Also listed are the local coupling strength metrics R and I determined from the scatter of evaporative fraction EF (BAEBBR measurement) relative to soil moisture SM (both SWATS and EBBR measurements). In addition, the inverse-distance weightings (IDW) relative to the CF are shown for each station. Finally, the last row lists the regional averages of the unweighted and weighted (in parentheses) R and I values across all the extended facility sites. In addition, for each R value the range of the estimated +/- 95-percent confidence limits also are given in brackets, assuming 148 independent samples for SWATS-EF, and 168 for EBBR-EF correlations.

Site	Location Soil, Vegetation Type	Distance to CF (km)	IDW	R, I SWATS	R, I EBBR
E4	Plevna, KS (38.0 N, 98.3 W) fine sandy loam, shrubs/grass	157.44	.101	.55 [.42 to .66], .062	.50 [.37 to .61], .058
E7	Elk Falls, KS (37.4 N, 96.2 W) silt loam, pasture	143.00	.111	.38 [.23 to .51], .038	.22 [.07 to .36], .022
E9	Ashton, KS (37.1 N, 97.2 W) loam, pasture	53.05	.306	.21 [.05 to .36], .022	.15 [-.01 to .30], .017
E12	Pawhuska, OK (36.7 N, 96.3 W) sandy loam, tallgrass prairie	108.88	.146	.090 [-.08 to .25],.008	.14 [-.01 to .29], .012
E15	Ringwood, OK (36.4 N, 98.2 W) sandy loam, pasture	70.68	.225	.33 [.17 to .47], .033	.28 [.13 to .42], .032
E20	Meeker, OK (35.5 N, 96.9 W) fine sandy loam, pasture	144.64	.110	.52 [.39 to .63], .059	.57 [.46 to .67], .064
Regional-average values:				R **=** .35 [.20 to .49], I = .037 R = .31 [.15 to .45], I = .034	(or R = .31 [.16 to .44], I = .032) for SWATS SM (or R = .27 [.12 to .41], I = .030) for EBBR SM

Table 4: The top panel lists the arithmetic average of the coupling strength metrics R and I associated with the SWATS, CO2FLX, and EBBR soil moisture measurements at the SGP-CF site (coordinates 36.61 N, 97.48 W). The bottom panel lists the corresponding R and I metrics for both the free-running AMIP and the controlled HC simulations at the closest model grid point to CF (coordinates 36.28 N, 97.50 W). For both observational and model results, the R and I values are computed from daily averages over months MJJA of the 2003-2011 period. In both cases also, the range of the +/- 2σ (95 percent) confidence levels on R are indicated in brackets, assuming 164 statistically independent pairings for the observational correlations and 221 for the model simulations (see Section 3.2.1 discussion).

Average Observed Coupling Strength	
SM-EF	R = .42 [.28 to .54] I = .053
SM-RH	R = .45 [.32 to .57] I = 5.86 %
SM-T	R = - .32 [-.17 to -.45] I = - 1.50 K

Model Coupling Strengths		
	AMIP	**HC**
SM-EF	R = .67 [.57 to .75] I = .13	R = .71 [.62 to .78] I = .10
SM-RH	R = .76 [.70 to .81] I = 15.6 %	R = .71 [.62 to .78] I = 12.0 %
SM-T	R = -.80 [-.75 to -.84] I = -4.45 K	R = -.53 [-.43 to -.62] I = -2.50 K

Table 5: Comparative performance statistics for AMIP (unshaded rows) and HC (shaded rows) simulations of the CAM5.1/CLM4 model at its closest grid point (coordinates 36.28 N, 97.50 W) to the SGP-CF site (coordinates 36.28 N, 97.50 W), with respect to ARM observations at the SGP-CF site, where all data are daily averages over the MJJA warm seasons of years 2003-2011. The listed statistics include each simulation's mean bias and root-mean-square error (RMSE) with respect to the observations, as well as the ratio of the modeled temporal variability to that of the observations (σ_m^2/σ_o^2).

Variable	Observed Mean	Model Mean	Mean Bias	RMSE	σ_m^2/σ_o^2
Precipitation Rate (mm day^{-1})	3.11	2.01	-1.04.	10.69	0.12
		2.77	-0.33	10.37	0.37
Sfc Net Downward Shortwave Flux (W m^{-2})	233.	222.	-11.	109.	0.67
		221.	-12.	88.	0.78
Sfc Net Upward Longwave Flux (W m^{-2})	62.	77.	+15.	40.	1.83
		69.	+7.	20.	1.46
Sfc Latent Heat Flux (W m^{-2})	101.	73.	-28.	70.	0.47
		96.	-5.	58.	0.52
Sfc Sensible Heat Flux (W m^{-2})	47.	57.	+10.	60.	0.55
		41.	-6.	54.	0.36
Sfc Evaporative Fraction	0.474	0.454	-.020	0.20	1.54
		0.536	+.062	0.16	1.20
Sfc Relative Humidity (%)	65.5	52.3	-13.2	26.0	2.76
		61.1	-4.4	11.7	1.67
Sfc Air Temperature (K)	297.3	301.5	+4.2	6.4	1.04
		299.5	+2.2	2.9	1.01
5-cm Soil Moisture, relative to SWATS (m^3/m^3)	0.283	0.234	-0.049	0.085	2.73
		0.281	-0.002	0.049	2.48
5-cm Soil Moisture, relative to CO2FLX (m^3/m^3)	0.178	0.234	+0.056	0.101	0.85
		0.281	+0.103	0.104	1.12

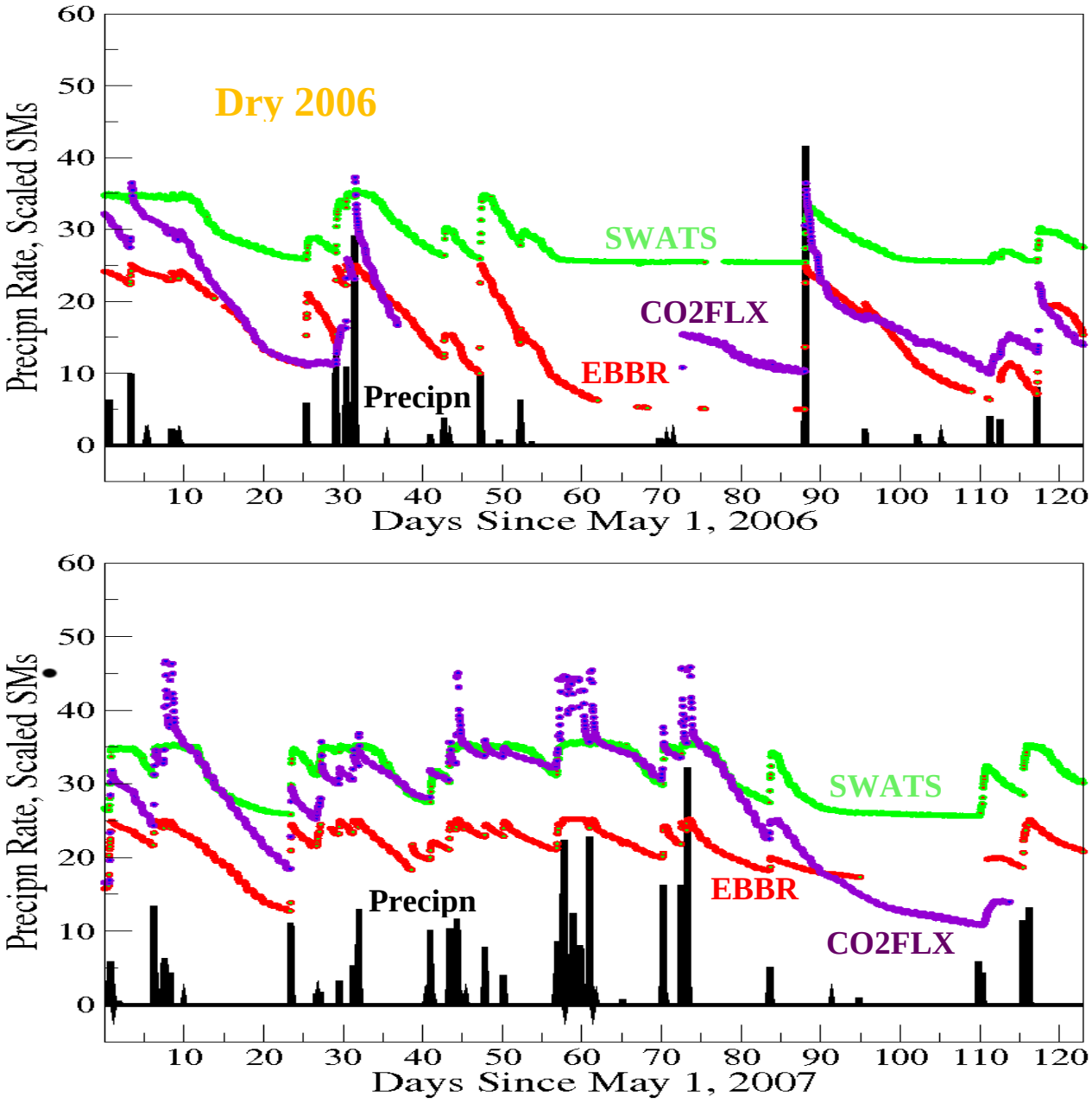

Figure 1: Time series of three independent measurements of shallow depth soil moisture SM at the SGP-CF site (coordinates 36.61 N, 97.48 W) in the anomalously dry 2006 MJJA (top) and in the anomalously wet 2007 MJJA season (bottom). In each year, precipitation rates are shown in black, SWATS 5-cm SM in green, EBBR 2.5-cm SM in red, and CO2FLX 5-cm SM in violet. Note: the SM values (in units of m^3/m^3) are multiplied by a factor of 100, so that they can be displayed on the same scale as the precipitation rate (in units of mm hr^{-1}).

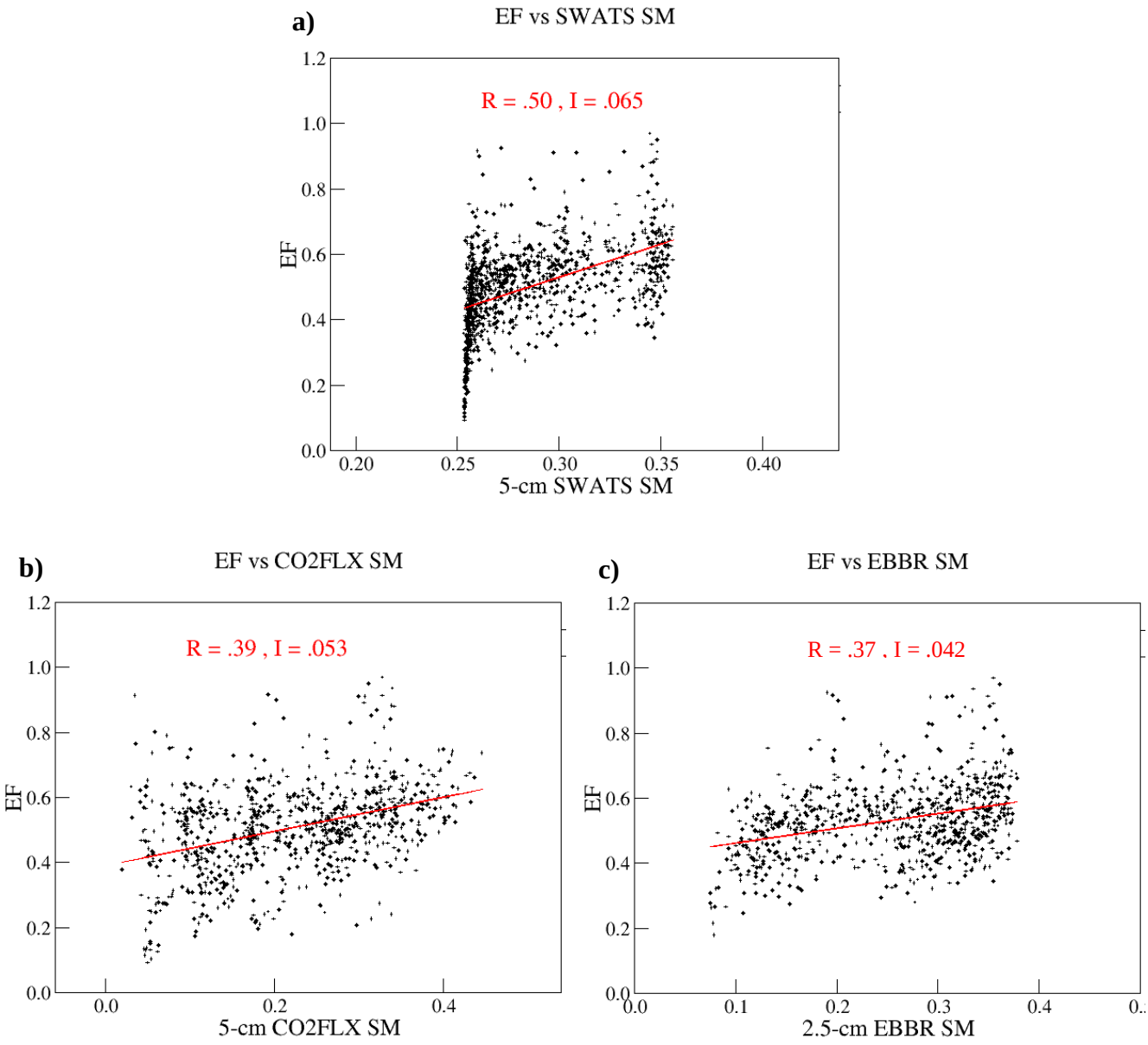

Figure 2: 2003-2011 MJJA daily average scatter of evaporative fraction EF, measured by the EBBR instrument, versus a) SWATS 5-cm depth soil moisture, b) CO2FLX 5-cm depth soil moisture, and c) EBBR 2.5-cm depth soil moisture, all observed at the SGP-CF site. SM values are in volumetric units of m^3/m^3 and EF is dimensionless. The coupling-strength metrics R and I are also shown in each case (consult Section 3 of the text for details).

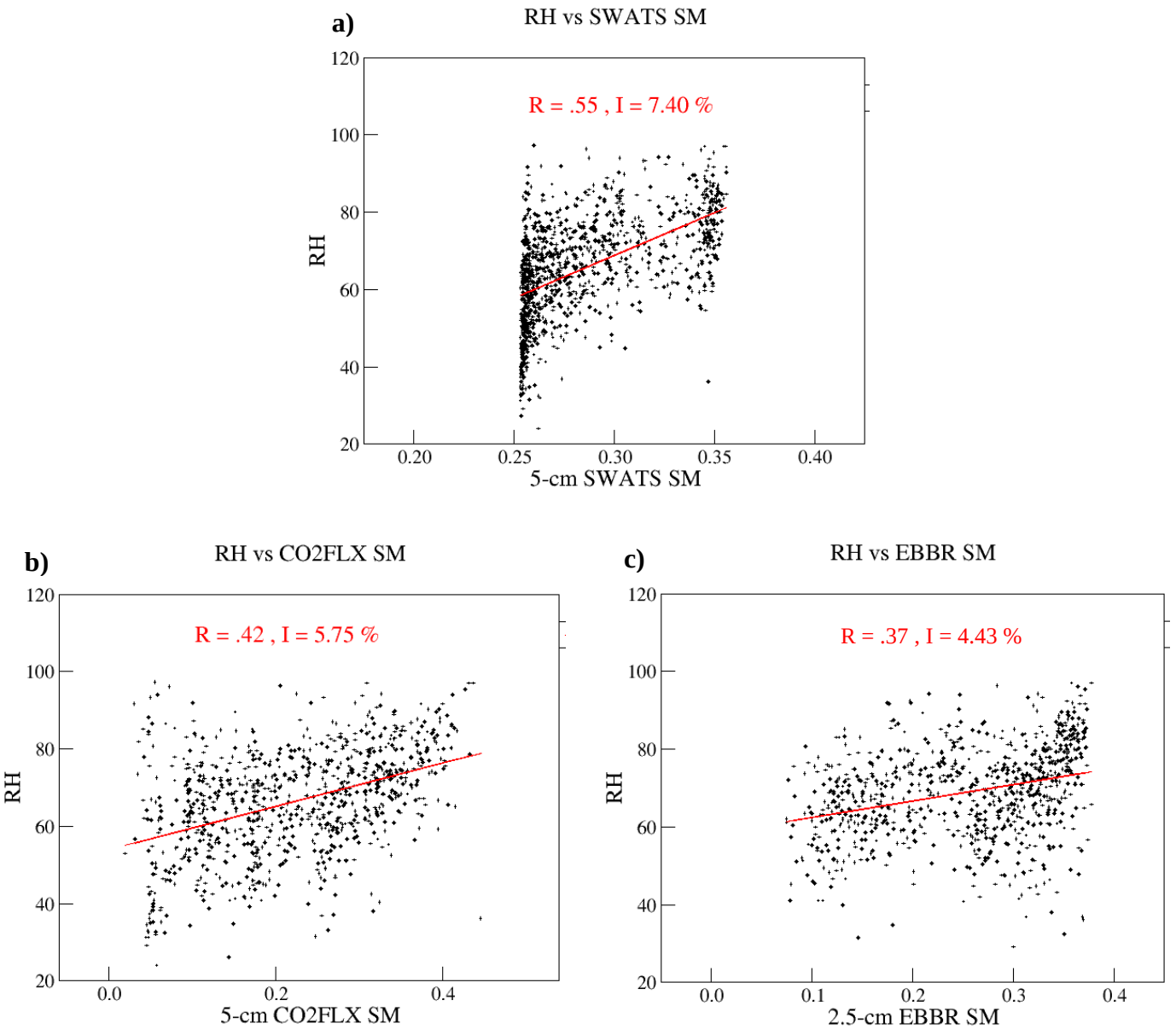

Figure 3: As in Figure 2, except for the daily average scatter of surface relative humidity RH (in %) plotted versus shallow-depth soil moisture (in m^3/m^3) given by a) SWATS, b) CO2FLX, and c) EBBR measurements, respectively.

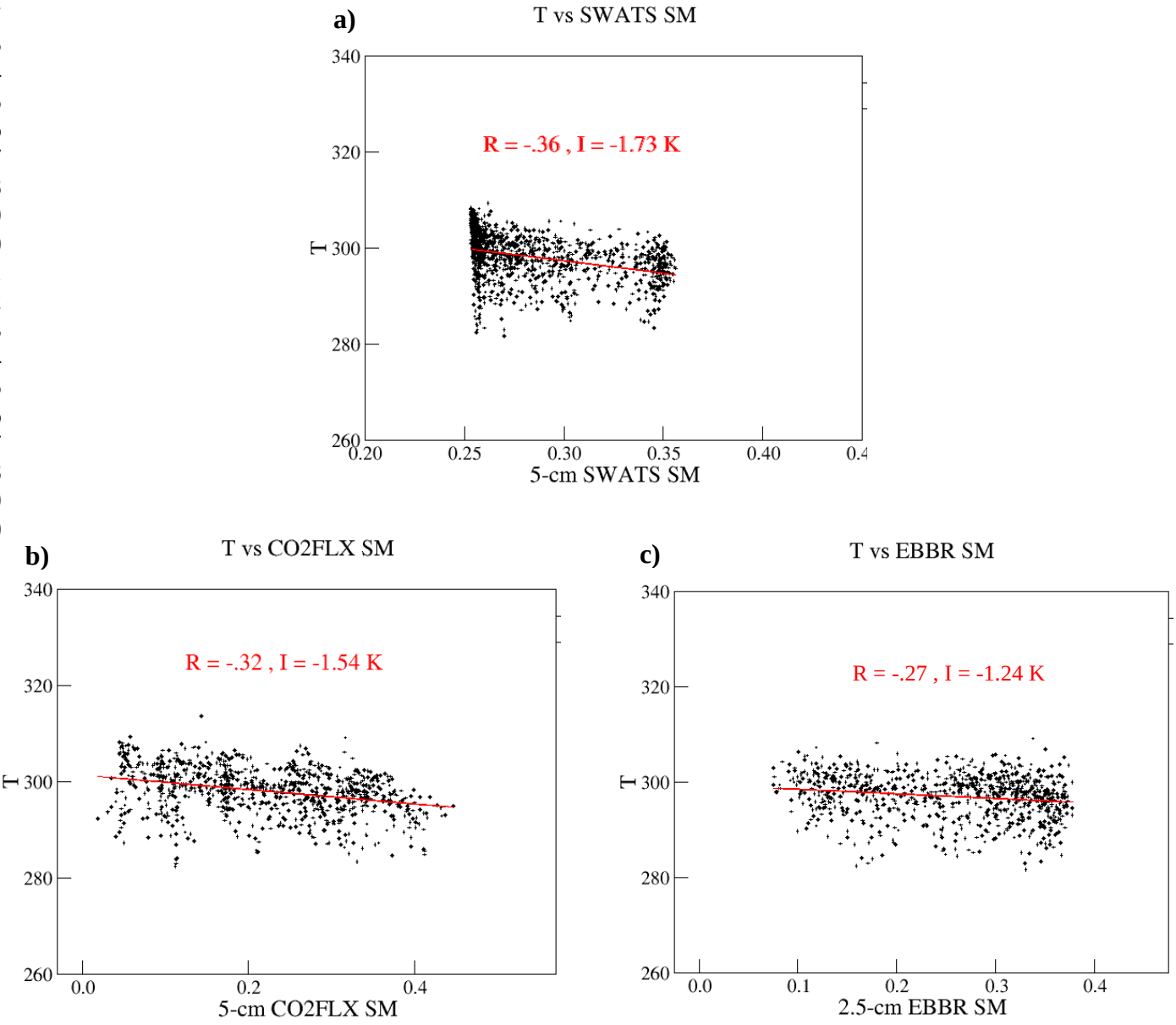

Figure 4: As in Figure 2, except for the scatter of daily average surface air temperature T (in K) plotted versus shallow-depth soil moisture given by the a) SWATS, b) CO2FLX, and c) EBBR measurements, respectively.

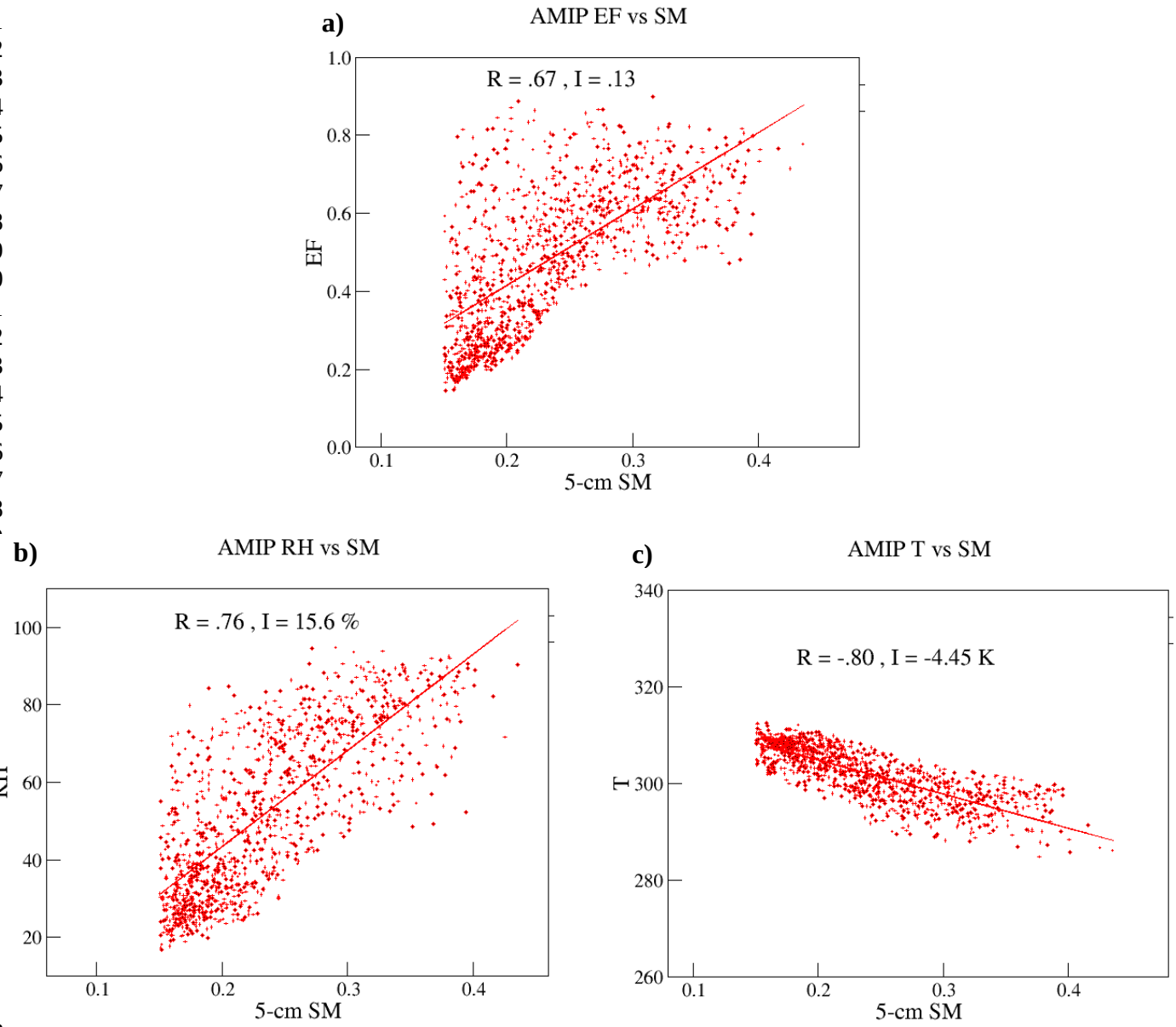

Figure 5: 2003-2011 MJJA daily average scatter of CAM5.1 surface atmospheric variables versus CLM4 soil moisture at 5-cm depth (in volumetric units of m^3/m^3) from the free-running AMIP simulation are shown. In a), the surface evaporative fraction EF versus model SM is displayed, while in b) and c), respectively, the model surface relative humidity RH (in %) and surface air temperature T (in K), both versus the model SM are shown. LAC strength metrics R and I are also displayed in each case.

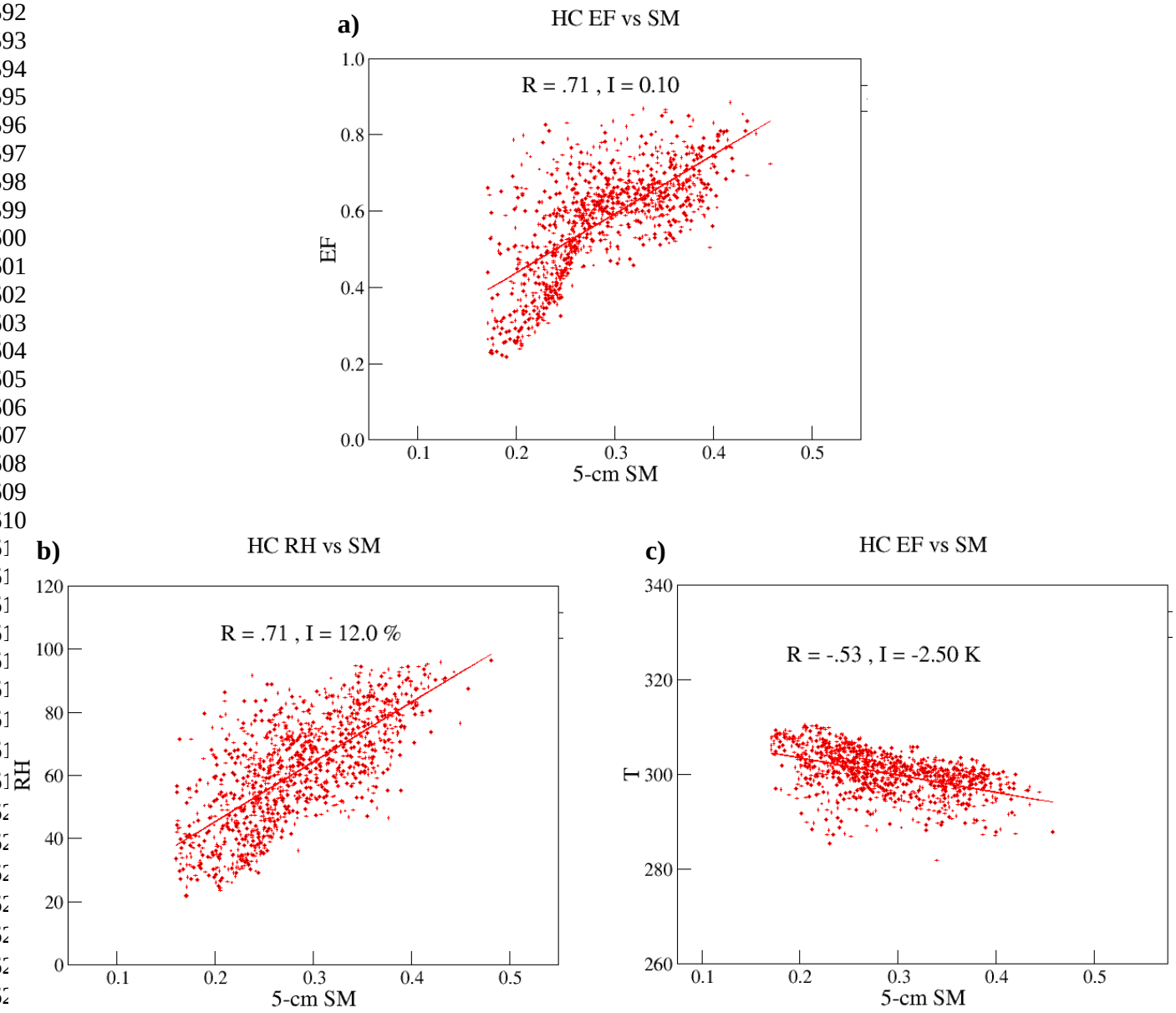

Figure 6: As in Figure 5, except for the controlled HC simulation of the CAM5.1/CLM4 model.

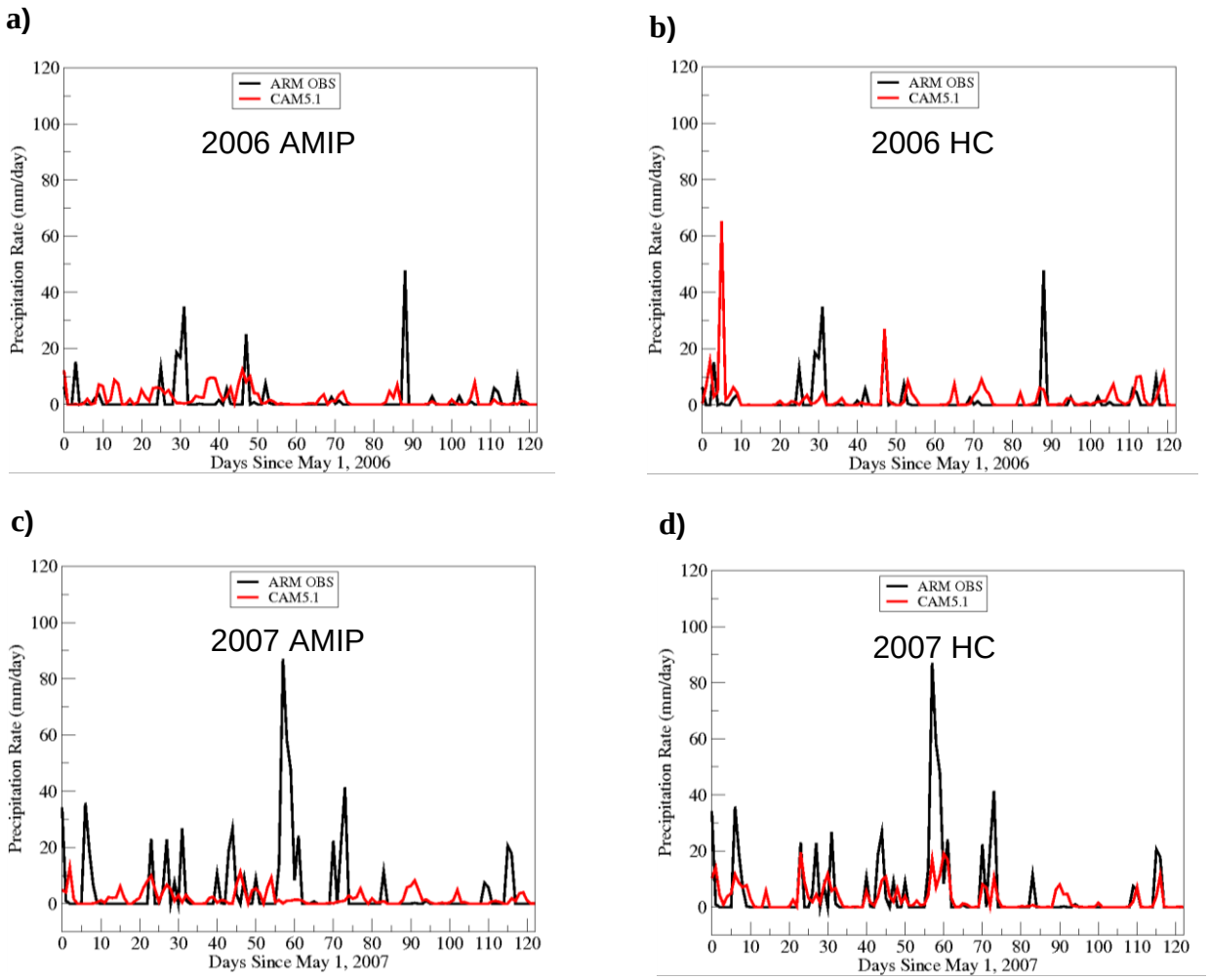

Figure 7: Time series of AMIP and HC simulations of daily average precipitation rate (in mm day^{-1}, red line) at the closest model grid point to the ARM SGP-CF site (coordinates 36.28 N, 97.50 W) during the MJJA season of relatively dry and wet years 2006/2007. These model results are compared with observations (black line) at the CF site (coordinates 36.61 N, 97.48 W) for the same time periods.

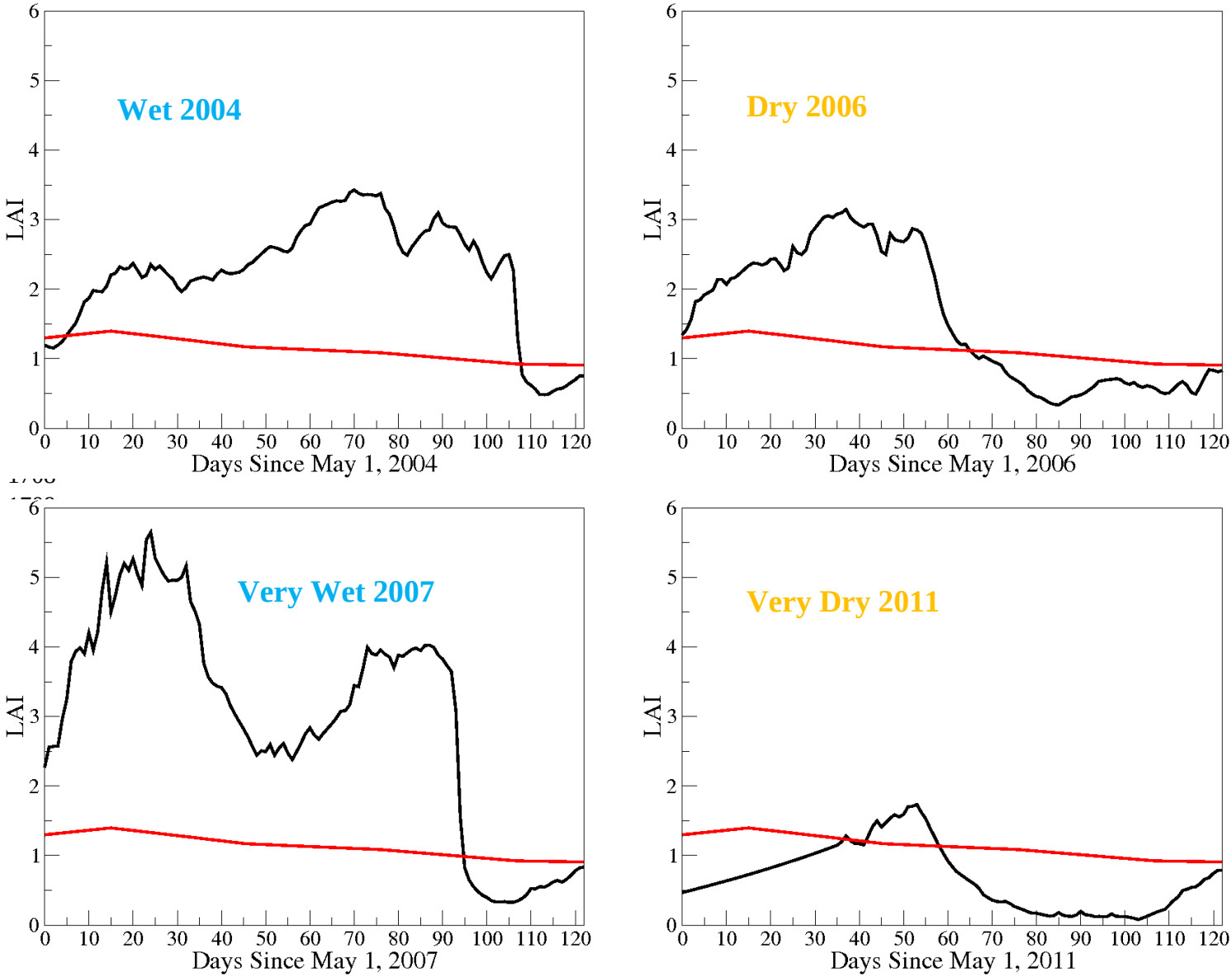

Figure 8: Observational estimates of leaf area index LAI (in dimensionless units) at the SGP-CF site (black lines) in years displaying diverse hydroclimatic conditions, compared with its representation in the controlled HC simulation of the CAM5.1/CLM4 model (red lines) in the same years.

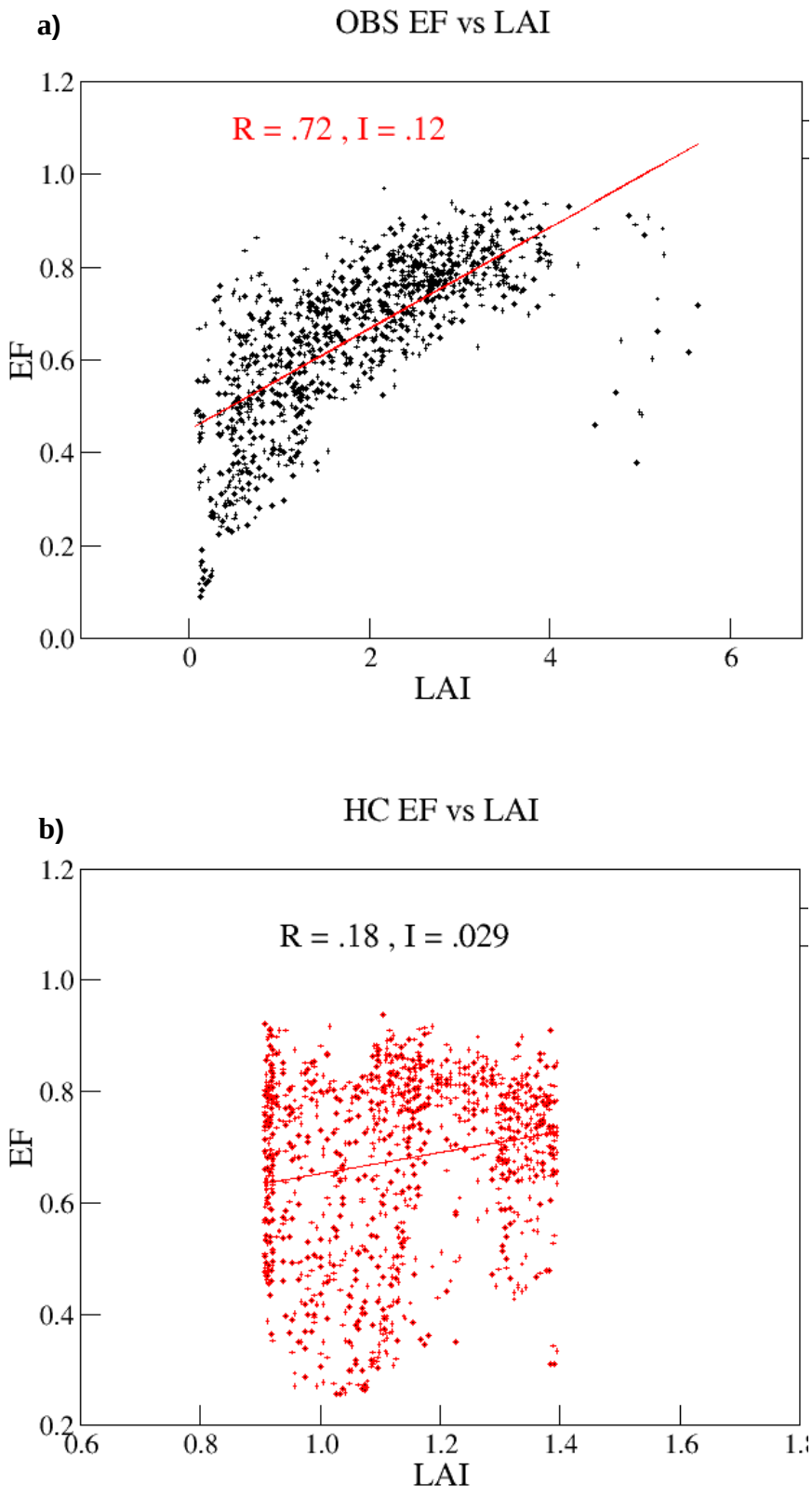

Figure 9: 2003-2011 MJJA scatter plots and estimated coupling-strength metrics R and I of daytime (12Z to 23 Z) averages of evaporative fraction EF versus leaf area index LAI, as observed a) at the SGP-CF site for grass land cover, and as simulated b) in the controlled HC experiment of the CAM5.1/CLM4 at the grid point closest to the SGP-CF site.

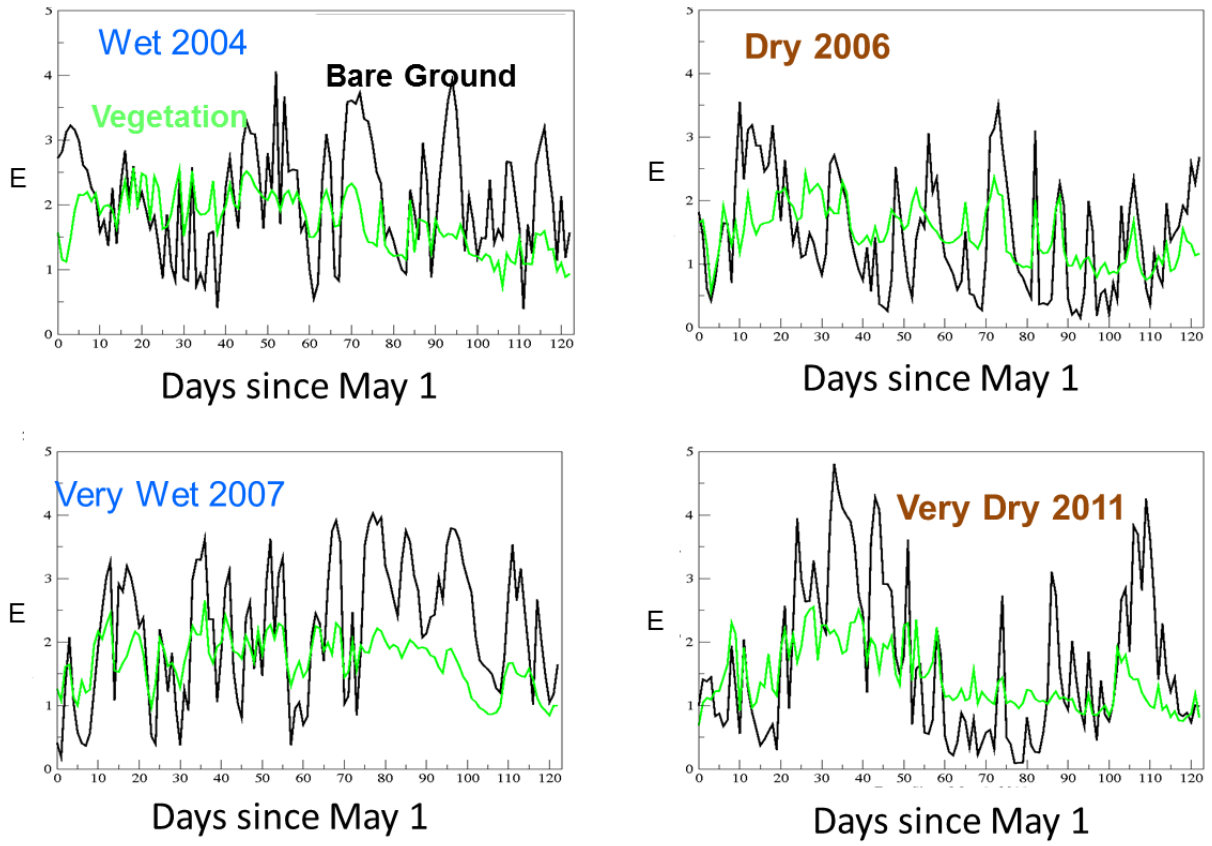

Figure 10: Contributions to surface evaporation E (in units of mm day^{-1}) by vegetation (in green) and by bare soil (in black) in the controlled HC simulation of the CAM5.1/CLM4 model, for the MJJA season in years displaying diverse hydroclimatic conditions. Note that the contributions by vegetation include both transpiration and canopy evaporation.